ResearchGate

See discussions, stats, and author profiles for this publication at: https://www.researchgate.net/publication/339345891

Rotation-Based Mixed Formulations for an Elasticity–Poroelasticity Interface Problem

Article *in* SIAM Journal on Scientific Computing · February 2020

DOI: 10.1137/19M1268343

CITATIONS
19

READS
246

5 authors, including:



Bryan Gómez Vargas
University of Costa Rica
20 PUBLICATIONS **153** CITATIONS
SEE PROFILE



David Mora
University of Bío-Bío
79 PUBLICATIONS **1,697** CITATIONS
SEE PROFILE



Ricardo Ruiz Baier
Monash University (Australia)
174 PUBLICATIONS **2,827** CITATIONS
SEE PROFILE

All content following this page was uploaded by Ricardo Ruiz Baier on 10 April 2020.

The user has requested enhancement of the downloaded file.

SIAM J. SCI. COMPUT.
Vol. 42, No. 1, pp. B225–B249
© 2020 Society for Industrial and Applied Mathematics

ROTATION-BASED MIXED FORMULATIONS FOR AN ELASTICITY-POROELASTICITY INTERFACE PROBLEM*

VERÓNICA ANAYA†, ZOA DE WIJN‡, BRYAN GÓMEZ-VARGAS§, DAVID MORA¶, AND RICARDO RUIZ-BAIER‖

Abstract. In this paper we introduce a new formulation for the stationary poroelasticity equations written using the rotation vector and the total fluid-solid pressure as additional unknowns, and we also write an extension to the elasticity-poroelasticity problem. The transmission conditions are imposed naturally in the weak formulation, and the analysis of the effective governing equations is conducted by an application of Fredholm's alternative. We also propose a monolithically coupled mixed finite element method for the numerical solution of the problem. Its convergence properties are rigorously derived and subsequently confirmed by a set of computational tests that include applications to subsurface flow in reservoirs as well as to dentistry-oriented problems.

Key words. elasticity-poroelasticity coupling, interface problems, Fredholm's alternative, mixed finite element method, error estimation

AMS subject classifications. 65N30, 74A50, 76S05, 74F10

DOI. 10.1137/19M1268343

1. Introduction.

The disparity of material properties across geometric interfaces is encountered in a wide variety of transmission problems arising in diverse scientific and engineering applications. This phenomenon is more clearly observed when the materials sharing the interface have intrinsically different features, such as an elastic medium in contact with a fluid or a poroelastic material in contact with an elastic one. For the latter, one specific example is the study of mechanical properties of the interaction between an oil reservoir and the surrounding nonpay rock. As mentioned in [23], the pore pressure variations and fluid content trapped in the cap rock are commonly not affected by outer injection or extraction of fluids in the reservoir. This fact motivates the use of partitioned models where one considers in the reservoir the classical Biot equations for poroelasticity, while the equations of linear elasticity suffice to describe the overall behavior of the cap rock (see also [45]). In this case, a careful setup of interface conditions is required. We refer the reader to

*Submitted to the journal's Computational Methods in Science and Engineering section June 14, 2019; accepted for publication (in revised form) October 23, 2019; published electronically February 18, 2020. This work was completed during a visit of the first, third, and fourth authors to the Mathematical Institute of the University of Oxford.

https://doi.org/10.1137/19M1268343

Funding: This work was partially supported by CONICYT-Chile through FONDECYT project 11160706, through the Becas-Chile Programme for foreign students, and through the project AFB170001 of the PIA Program Concurso Apoyo a Centros Científicos y Tecnológicos de Excelencia con Financiamiento Basal; and by the Oxford Centre for Doctoral Training in Industrially Focused Mathematical Modelling.

†GIMNAP, Departamento de Matemática, Universidad del Bío-Bío, Concepción, Chile (vanaya@ubiobio.cl).

‡Mathematical Institute, University of Oxford, Oxford OX2 6GG, UK (dewijn@maths.ox.ac.uk).

§Sección de Matemática, Sede de Occidente, Universidad de Costa Rica, San Ramón, Costa Rica, and CI^{2}MA & Departamento de Ingeniería Matemática, Universidad de Concepción, Concepción, Chile (bryan.gomezvargas@ucr.ac.cr).

¶GIMNAP, Departamento de Matemática, Universidad del Bío-Bío, Concepción, Chile, and CI^{2}MA, Universidad de Concepción, Concepción, Chile (dmora@ubiobio.cl).

‖Corresponding author. Mathematical Institute, University of Oxford, Oxford OX2 6GG, UK, and Universidad Adventista de Chile, Casilla 7-D, Chillán, Chile (ruizbaier@maths.ox.ac.uk).

[43, 37] for a detailed discussion on the physical and mathematical implications of these transmission terms.

Some other applications of elastic-poroelastic coupled systems include the reservoir modeling mentioned above, the classical problem of soil-structure interaction (which can include soil-retaining walls and shallow foundations [34] or the earth's crustal deformation [39]), the simulation of periodontal ligament-tooth contact as done in [18], the development of noise reduction for aircraft design using acoustic-elastic wave propagation [28, 42], and the study of low-friction cartilage tissue in vertebrates [14].

The mathematical properties of these types of models have been addressed in [23]. There, the authors develop a solvability theory for the semidiscrete elastic and poroelastic subproblems, making use of a Galerkin method combined with compactness arguments permitting the passage to the limit.

In contrast, the specific version of the model we analyze here uses a modification of the recent displacement-rotation-pressure formulation of elasticity equations proposed in [4], together with a new formulation for the equations of poromechanics written in terms of displacement, fluid pressure, rotation, and total pressure. Our model assumes that the elastic domain is completely clamped on its exterior boundary, whereas on the interface between the poroelastic and elastic media we impose continuity of displacement, zero fluid flux, and a transmission condition related to the continuity of total traction forces written in terms of tangential rotations and pressure. The mathematical structure of the set of equations and interface conditions reveals that the system is written as a monolithic coupling, where the interface continuity conditions stated above are incorporated naturally through the weak formulation, without the need of additional Lagrange multipliers. In particular, the regularity of the displacement and the scaling of the momentum equations in both domains allow us to consider a global displacement. The well-posedness of the continuous problem is studied by grouping the unknowns with compatible regularity and realizing that the resulting problem is a mixed variational formulation resembling the system introduced in [38] that describes the Biot equations in their displacement-pressure-total pressure formulation and which is analyzed using Fredholm's alternative. Our analysis also discusses the limit case when the specific storage coefficient in the poroelastic domain goes to zero, and we observe that the continuous dependence on data is robust with respect to the Lamé constants of the solids in both regions of the domain.

A similar framework is established for the discrete problem, here defined for Galerkin schemes with arbitrary order. For example, we can employ piecewise quadratic and continuous approximations for displacements in the whole domain and for fluid pressure in the poroelastic medium, whereas piecewise linear and discontinuous approximations are employed for all remaining unknowns (rotations in both domains, total pressure in the poroelastic domain, and solid pressure in the elastic domain). For this particular scheme our error estimates predict an overall second-order accuracy, and the involved bounds are also robust with respect to the Lamé constants of the solids. Let us emphasize that the literature related to numerical methods for the coupling of elasticity and poroelasticity is still quite restricted. We are only aware of the conforming Galerkin scheme presented in [23], where a domain decomposition on the interface between the two subdomains is done by means of discontinuous Galerkin jumps and mortar terms; the stability of a mixed variant for that formulation, recently analyzed in [25]; the primal method combined with stochastic parameter estimation advanced in [45]; and the loosely coupled segregated approaches developed for a fluid-poromechanics interaction problem studied in [10].

Let us stress that the advantages of using rotations are shared with a wide class of previous formulations for general elastic materials. They relate to the direct approximation of the rotation vector but without the need for constraining its rotation to coincide with that of the medium. Also, they can be of special applicability for nonpolar media and the modeling of helicoidal motion (see, e.g., [6, 35, 36, 31] and the references therein). However, in our case the main motivation comes from the PDE and numerical analysis aspects of the resulting formulations, since they resemble the vorticity-based equations for incompressible flow in classical and contemporary works including, e.g., [26, 40, 24, 15, 41, 13, 1, 17, 8, 16, 3, 5]. The theoretical analyses of these two very different families of models have remarkable connections.

The contents of this paper will be presented in the following manner. Section 2 defines the model problem in strong form, specifying the boundary and interface conditions. It also includes the derivation of an appropriate weak formulation, and the statement of preliminary properties of the involved bilinear forms. The existence and uniqueness of weak solutions is then studied in section 3. This analysis is mainly based on Fredholm's alternative and saddle-point theorems, where we also establish continuous dependence on data, with bounds that turn out to be robust with respect to the elasticity parameters intrinsic to each subdomain. A suitable Galerkin method, together with finite element spaces, will be defined in section 4. This section also incorporates the analysis of well-posedness of the discrete problem, the proof of a quasi-optimality result, and the derivation of a priori error bounds. We close in section 5 with a few computational examples that serve to confirm the accuracy of the mixed finite element method and to illustrate the suitability of the model and of the family of schemes in some applicative problems.

2. Set of governing equations.

2.1. Model problem and boundary-transmission conditions. Let us consider a bounded Lipschitz domain $\Omega \subset \mathbb{R}^d$, $d \in \{2, 3\}$, in conjunction with a partition into nonoverlapping and connected subdomains Ω^{E}, Ω^{P} representing zones of nonpay rock (where we will set the equations of linear elasticity) and a reservoir (where we aim at solving the poroelasticity equations), respectively. We also assume that the reservoir is completely immersed in the overall domain, that is, $\overline{\Omega^{\mathrm{P}}} \subset \Omega$, such that the interface between the two subdomains, denoted as $\Sigma = \partial\Omega^{\mathrm{P}} \cap \partial\Omega^{\mathrm{E}}$, coincides with the boundary of the pay zone, as portrayed in Figure 2.1. Note that on the interface, we consider that the normal unit vector $\boldsymbol{n}$ is pointing from Ω^{P} to Ω^{E}.

In the reservoir, we consider the steady form of the balance laws for the poroelasticity equations (see, for instance, [7], and see [38, 32, 33] for the stationary case), i.e., find the displacement $\boldsymbol{u}^{\mathrm{P}}$ and the pore pressure of the fluid p^{P} such that

$$-\mu^{\mathrm{P}}\Delta\boldsymbol{u}^{\mathrm{P}} - (\lambda^{\mathrm{P}} + \mu^{\mathrm{P}})\nabla\,\mathrm{div}(\boldsymbol{u}^{\mathrm{P}}) + \alpha\nabla p^{\mathrm{P}} = \widetilde{\boldsymbol{f}}^{\mathrm{P}} \qquad \text{in } \Omega^{\mathrm{P}}, \tag{2.1}$$

$$c_0 p^{\mathrm{P}} + \alpha\,\mathrm{div}(\boldsymbol{u}^{\mathrm{P}}) - \frac{1}{\xi}\,\mathrm{div}\left[\kappa(\nabla p^{\mathrm{P}} - \rho\boldsymbol{g})\right] = s^{\mathrm{P}} \qquad \text{in } \Omega^{\mathrm{P}}, \tag{2.2}$$

where s^{P} is a smooth fluid source term; κ is the permeability of the porous matrix constituting the reservoir (here assumed isotropic and satisfying $0 < \kappa_1 \leq \kappa(\boldsymbol{x}) \leq \kappa_2 < \infty$ for all $\boldsymbol{x} \in \Omega^{\mathrm{P}}$); $\lambda^{\mathrm{P}}, \mu^{\mathrm{P}}$ are the Lamé constants of the solid Ω^{P} (dilation and shear moduli of elasticity, respectively); $c_0 > 0$ is the constrained specific storage coefficient; $\alpha > 0$ is the Biot–Willis parameter, $\boldsymbol{g}$ is the gravity acceleration, and $\xi > 0, \rho > 0$ are the viscosity and density of the pore fluid, respectively. Next, for the poroelasticity problem, we propose a new four-field variational formulation. In fact,

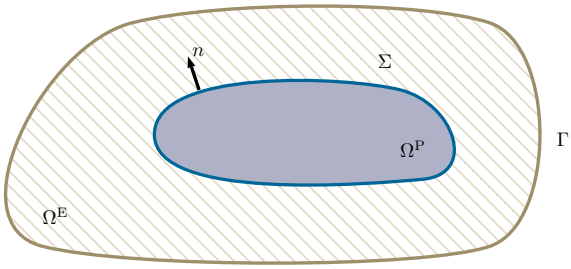


FIG. 2.1. *Sketch of the multidomain configuration.*

we begin by introducing the additional unknowns

$$\phi^{\mathrm{P}} := \alpha(\lambda^{\mathrm{P}}+\mu^{\mathrm{P}})^{-1}p^{\mathrm{P}} - (1+\eta^{\mathrm{P}})\,\mathrm{div}(\boldsymbol{u}^{\mathrm{P}}) \quad \text{and} \quad \boldsymbol{\omega}^{\mathrm{P}} := \sqrt{\eta^{\mathrm{P}}}\,\mathbf{curl}\,\boldsymbol{u}^{\mathrm{P}}, \tag{2.3}$$

where the first one can be regarded as a rescaled total pressure or volumetric stress, and the second one corresponds to the rescaled rotations, with the auxiliary scaling parameter $\eta^{\mathrm{P}} := \frac{\mu^{\mathrm{P}}}{\lambda^{\mathrm{P}}+\mu^{\mathrm{P}}}$. In this way, the identities in (2.3) in combination with (2.1)–(2.2) give rise to the following four-field formulation for the poroelasticity problem: find the displacement $\boldsymbol{u}^{\mathrm{P}}$, the poroelastic rotation vector $\boldsymbol{\omega}^{\mathrm{P}}$, the pore fluid pressure p^{P}, and the rescaled total poroelastic pressure ϕ^{P} such that

$$\sqrt{\eta^{\mathrm{P}}}\,\mathbf{curl}\,\boldsymbol{\omega}^{\mathrm{P}} + \nabla\phi^{\mathrm{P}} = \boldsymbol{f}^{\mathrm{P}} \quad \text{in } \Omega^{\mathrm{P}}, \tag{2.4}$$

$$\boldsymbol{\omega}^{\mathrm{P}} - \sqrt{\eta^{\mathrm{P}}}\,\mathbf{curl}\,\boldsymbol{u}^{\mathrm{P}} = \mathbf{0} \quad \text{in } \Omega^{\mathrm{P}}, \tag{2.5}$$

$$(1+\eta^{\mathrm{P}})^{-1}\phi^{\mathrm{P}} + \mathrm{div}(\boldsymbol{u}^{\mathrm{P}}) - \alpha(1+\eta^{\mathrm{P}})^{-1}(\lambda^{\mathrm{P}}+\mu^{\mathrm{P}})^{-1}p^{\mathrm{P}} = 0 \quad \text{in } \Omega^{\mathrm{P}}, \tag{2.6}$$

$$\big[c_0 + \alpha^2(\mu^{\mathrm{P}}+\lambda^{\mathrm{P}})^{-1}(1+\eta^{\mathrm{P}})^{-1}\big]p^{\mathrm{P}} - \alpha(1+\eta^{\mathrm{P}})^{-1}\phi^{\mathrm{P}} - \frac{1}{\xi}\,\mathrm{div}\,\big[\kappa(\nabla p^{\mathrm{P}} - \rho\boldsymbol{g})\big] = s^{\mathrm{P}} \quad \text{in } \Omega^{\mathrm{P}}, \tag{2.7}$$

where the right-hand side has been rescaled as $\boldsymbol{f}^{\mathrm{P}} := \frac{1}{\lambda^{\mathrm{P}}+\mu^{\mathrm{P}}}\widetilde{\boldsymbol{f}}^{\mathrm{P}}$.

In Ω^{E} the governing equations correspond to the system of linear elasticity written in terms of displacement $\boldsymbol{u}^{\mathrm{E}}$, elastic pressure p^{E}, and elastic rotation vector $\boldsymbol{\omega}^{\mathrm{E}} := \sqrt{\eta^{\mathrm{E}}}\,\mathbf{curl}\,\boldsymbol{u}^{\mathrm{E}}$ associated with the nonpay zone:

$$\sqrt{\eta^{\mathrm{E}}}\,\mathbf{curl}\,\boldsymbol{\omega}^{\mathrm{E}} + \nabla p^{\mathrm{E}} = \boldsymbol{f}^{\mathrm{E}} \quad \text{in } \Omega^{\mathrm{E}}, \tag{2.8}$$

$$\boldsymbol{\omega}^{\mathrm{E}} - \sqrt{\eta^{\mathrm{E}}}\,\mathbf{curl}\,\boldsymbol{u}^{\mathrm{E}} = 0 \quad \text{in } \Omega^{\mathrm{E}}, \tag{2.9}$$

$$\mathrm{div}\,\boldsymbol{u}^{\mathrm{E}} + p^{\mathrm{E}} = 0 \quad \text{in } \Omega^{\mathrm{E}}, \tag{2.10}$$

where $\eta^{\mathrm{E}} := \frac{\mu^{\mathrm{E}}}{2\mu^{\mathrm{E}}+\lambda^{\mathrm{E}}} > 0$ is a scaling parameter depending on the Lamé constants of the elastic nonpay rock Ω^{E}, and $\boldsymbol{f}^{\mathrm{E}}$ corresponds to the rescaled function $\boldsymbol{f}^{\mathrm{E}} := \frac{1}{2\mu^{\mathrm{E}}+\lambda^{\mathrm{E}}}\widetilde{\boldsymbol{f}}^{\mathrm{E}}$.

Remark 2.1. An important consideration here is that such a scaling is different from that used in [4]. As we will see in section 2.2, this choice makes convenient the balancing of bilinear forms corresponding to similar terms at the moment of casting the governing equations in weak form, especially regarding the contributions on the interface.

Regarding boundary conditions, we assume here that on the external boundary of the nonpay rock the displacements are zero,

$$\boldsymbol{u}^{\mathrm{E}} = \mathbf{0} \quad \text{on} \quad \Gamma, \tag{2.11}$$

and the system is closed by setting suitable transmission conditions on the interface between the reservoir and the nonpay zone,

$$\boldsymbol{u}^{\mathrm{P}} = \boldsymbol{u}^{\mathrm{E}}, \quad \sqrt{\eta^{\mathrm{P}}}\,\boldsymbol{\omega}^{\mathrm{P}} \times \boldsymbol{n} + \phi^{\mathrm{P}}\boldsymbol{n} = \sqrt{\eta^{\mathrm{E}}}\,\boldsymbol{\omega}^{\mathrm{E}} \times \boldsymbol{n} + p^{\mathrm{E}}\boldsymbol{n}, \quad \frac{\kappa}{\xi}(\nabla p^{\mathrm{P}} - \rho\boldsymbol{g}) \cdot \boldsymbol{n} = 0, \quad \text{on} \quad \Sigma, \tag{2.12}$$

which represent continuity of the medium, a generalized relation for the matching of total normal stresses, and no-flux of fluid at the interface, respectively. The second condition in (2.12) can be linked to the generalized Navier condition used in fluids

$$[\boldsymbol{\epsilon}(\boldsymbol{u}^{\mathrm{P}})\boldsymbol{n}]_{\tau} + \Lambda \boldsymbol{u}^{\mathrm{P}} = \mathbf{0},$$

where the subscript τ denotes the vectorial tangential trace of any vector, defined by $\boldsymbol{v}_{\tau} := \boldsymbol{v} - (\boldsymbol{v} \cdot \boldsymbol{n})\boldsymbol{n}$, and Λ is a type (1,1) tensor defined on Σ [22]. In the simple case when $\Lambda = \delta \mathbf{I}$ (with δ a positive or negative friction coefficient), one retrieves a Navier-type friction transmission condition. If Λ is instead the Weingarten shape operator on the interface, this results in a continuity condition for the tangential rotations and the normal total pressure. Similar ideas can be found in, e.g., [22, 2, 12, 29, 11, 43, 19] for Navier–Stokes/Darcy and Brinkman–Darcy couplings, vascular Stokes–Darcy models, Lagrangian–Eulerian fluid-elastic transmission, time-harmonic elastic waves, and interface poromechanics, respectively. The last transmission condition imposes no leakage between the bodies as they are compressed, which implies mass conservation [14]. The balancing of scales in these interface conditions is a consequence of the rescaling highlighted in Remark 2.1.

2.2. Weak formulation. In order to derive a weak formulation for the system (2.4)–(2.12), we start by multiplying each equation of the poroelasticity problem by suitable test functions, integrating by parts whenever adequate (see (2.15)–(2.16)), and applying the second and third transmission conditions given in (2.12) to obtain

$$\begin{aligned}
&-\sqrt{\eta^{\mathrm{P}}}\int_{\Omega^{\mathrm{P}}} \mathbf{curl}\,\boldsymbol{v}^{\mathrm{P}} \cdot \boldsymbol{\omega}^{\mathrm{P}} + \int_{\Omega^{\mathrm{P}}} \phi^{\mathrm{P}} \mathrm{div}(\boldsymbol{v}^{\mathrm{P}}) - \langle \sqrt{\eta^{\mathrm{E}}}\,\boldsymbol{\omega}^{\mathrm{E}} \times \boldsymbol{n} + p^{\mathrm{E}}\boldsymbol{n}, \boldsymbol{v}^{\mathrm{P}} \rangle_{\Sigma} = -\int_{\Omega^{\mathrm{P}}} \boldsymbol{f}^{\mathrm{P}} \cdot \boldsymbol{v}^{\mathrm{P}}, \\
&\int_{\Omega^{\mathrm{P}}} \boldsymbol{\omega}^{\mathrm{P}} \cdot \boldsymbol{\theta}^{\mathrm{P}} - \sqrt{\eta^{\mathrm{P}}}\int_{\Omega^{\mathrm{P}}} \boldsymbol{\theta}^{\mathrm{P}} \cdot \mathbf{curl}\,\boldsymbol{u}^{\mathrm{P}} = 0, \\
&(1+\eta^{\mathrm{P}})^{-1}\int_{\Omega^{\mathrm{P}}} \phi^{\mathrm{P}}\psi^{\mathrm{P}} + \int_{\Omega^{\mathrm{P}}} \psi^{\mathrm{P}}\,\mathrm{div}(\boldsymbol{u}^{\mathrm{P}}) - \alpha(1+\eta^{\mathrm{P}})^{-1}(\lambda^{\mathrm{P}} + \mu^{\mathrm{P}})^{-1}\int_{\Omega^{\mathrm{P}}} p^{\mathrm{P}}\psi^{\mathrm{P}} = 0, \\
&-\left[c_0 + \alpha^2(\mu^{\mathrm{P}} + \lambda^{\mathrm{P}})^{-1}(1+\eta^{\mathrm{P}})^{-1}\right]\int_{\Omega^{\mathrm{P}}} p^{\mathrm{P}} q^{\mathrm{P}} \\
&+ \alpha(1+\eta^{\mathrm{P}})^{-1}\int_{\Omega^{\mathrm{P}}} \phi^{\mathrm{P}} q^{\mathrm{P}} - \xi^{-1}\int_{\Omega^{\mathrm{P}}} \kappa \nabla p^{\mathrm{P}} \cdot \nabla q^{\mathrm{P}} \\
&\qquad = -\rho\xi^{-1}\int_{\Omega^{\mathrm{P}}} \kappa \boldsymbol{g} \cdot \nabla q^{\mathrm{P}} - \int_{\Omega^{\mathrm{P}}} s^{\mathrm{P}} q^{\mathrm{P}}
\end{aligned} \tag{2.13}$$

for each $(\boldsymbol{v}^{\mathrm{P}}, \boldsymbol{\theta}^{\mathrm{P}}, \psi^{\mathrm{P}}, q^{\mathrm{P}}) \in \mathbf{H}^1(\Omega^{\mathrm{P}}) \times \mathbf{L}^2(\Omega^{\mathrm{P}}) \times \mathrm{L}^2(\Omega^{\mathrm{P}}) \times \mathrm{H}^1(\Omega^{\mathrm{P}})$. In turn, for (2.8)–(2.10) we proceed as in the mixed displacement-rotation-pressure formulation for

linear elasticity introduced in [4], and we obtain

$$
\begin{aligned}
-\sqrt{\eta^{\mathrm{E}}}\int_{\Omega^{\mathrm{E}}}\boldsymbol{\omega}^{\mathrm{E}}\cdot\mathbf{curl}\,\boldsymbol{v}^{\mathrm{E}}+\int_{\Omega^{\mathrm{E}}}p^{\mathrm{E}}\,\mathrm{div}(\boldsymbol{v}^{\mathrm{E}})+\langle\sqrt{\eta^{\mathrm{E}}}\,\boldsymbol{\omega}^{\mathrm{E}}\times\boldsymbol{n}+p^{\mathrm{E}}\boldsymbol{n},\boldsymbol{v}^{\mathrm{E}}\rangle_{\Sigma}&=-\int_{\Omega^{\mathrm{E}}}\boldsymbol{f}^{\mathrm{E}}\cdot\boldsymbol{v}^{\mathrm{E}},\\
\int_{\Omega^{\mathrm{E}}}\boldsymbol{\omega}^{\mathrm{E}}\cdot\boldsymbol{\theta}^{\mathrm{E}}-\sqrt{\eta^{\mathrm{E}}}\int_{\Omega^{\mathrm{E}}}\boldsymbol{\theta}^{\mathrm{E}}\cdot\mathbf{curl}\,\boldsymbol{u}^{\mathrm{E}}&=0,\\
\int_{\Omega^{\mathrm{E}}}q^{\mathrm{E}}\mathrm{div}(\boldsymbol{u}^{\mathrm{E}})+\int_{\Omega^{\mathrm{E}}}p^{\mathrm{E}}q^{\mathrm{E}}&=0
\end{aligned}
\tag{2.14}
$$

for each $(\boldsymbol{v}^{\mathrm{E}},\boldsymbol{\theta}^{\mathrm{E}},q^{\mathrm{E}})\in\mathbf{H}^1_{\Gamma}(\Omega^{\mathrm{E}})\times\mathbf{L}^2(\Omega^{\mathrm{E}})\times\mathrm{L}^2(\Omega^{\mathrm{E}})$, where

$$
\mathbf{H}^1_{\Gamma}(\Omega^{\mathrm{E}}):=\{\boldsymbol{v}^{\mathrm{E}}\in\mathbf{H}^1(\Omega^{\mathrm{E}}):\quad\boldsymbol{v}^{\mathrm{E}}=\mathbf{0}\quad\text{on}\quad\Gamma\}.
$$

Recall that, according to [24, Theorem 2.11], for a generic domain Ω, the relevant integration by parts formula corresponds to

$$
\int_{\Omega}\mathbf{curl}\,\boldsymbol{\omega}\cdot\boldsymbol{v}=\int_{\Omega}\boldsymbol{\omega}\cdot\mathbf{curl}\,\boldsymbol{v}+\langle\boldsymbol{\omega}\times\boldsymbol{n},\boldsymbol{v}\rangle_{\partial\Omega}
\tag{2.15}
$$

if $\Omega\subseteq\mathbb{R}^3$, or to

$$
\int_{\Omega}\mathbf{curl}\,\omega\cdot\boldsymbol{v}=\int_{\Omega}\omega\,\mathrm{rot}\,\boldsymbol{v}-\langle\boldsymbol{v}\cdot\boldsymbol{t},\omega\rangle_{\partial\Omega}
\tag{2.16}
$$

in 2D, where $\boldsymbol{t}$ is the tangent vector.

The first transmission condition in (2.12), together with the regularity of the solid displacements on each subdomain (to be specified below), implies that we can consider a single displacement field $\boldsymbol{u}$ and test function $\boldsymbol{v}$. That is the reason why the duality pairings between $\mathrm{H}^{-1/2}(\Sigma)$ and $\mathrm{H}^{1/2}(\Sigma)$ (represented by $\langle\cdot,\cdot\rangle_{\Sigma}$) disappear when we add the first row in (2.14) to the first row in (2.13). Furthermore, from now on we regard the poroelastic and elastic rotation vectors $\boldsymbol{\omega}^{\mathrm{P}}$ and $\boldsymbol{\omega}^{\mathrm{E}}$, respectively, the rescaled total poroelastic pressure ϕ^{P}, and the pressure p^{E} in the elastic domain as a single auxiliary unknown, namely $\vec{\boldsymbol{\omega}}:=(\boldsymbol{\omega}^{\mathrm{P}},\phi^{\mathrm{P}},\boldsymbol{\omega}^{\mathrm{E}},p^{\mathrm{E}})$ (defined in an appropriate product functional space) such that we can establish the well-posedness of the mixed variational formulation of interest using Fredholm's alternative theory for compact operators. Under this assumption, we arrive at the following: find $(\vec{\boldsymbol{\omega}},\boldsymbol{u},p^{\mathrm{P}})\in\mathbf{H}\times\mathbf{V}\times\mathrm{Q}^{\mathrm{P}}$ such that

$$
a(\vec{\boldsymbol{\omega}},\vec{\boldsymbol{\theta}})+b_1(\vec{\boldsymbol{\theta}},\boldsymbol{u})-b_2(\vec{\boldsymbol{\theta}},p^{\mathrm{P}})=0\qquad\forall\,\vec{\boldsymbol{\theta}}\in\mathbf{H},
\tag{2.17}
$$

$$
b_1(\vec{\boldsymbol{\omega}},\boldsymbol{v})=F(\boldsymbol{v})\qquad\forall\,\boldsymbol{v}\in\mathbf{V},
\tag{2.18}
$$

$$
b_3(\vec{\boldsymbol{\omega}},q^{\mathrm{P}})-c(p^{\mathrm{P}},q^{\mathrm{P}})=G(q^{\mathrm{P}})\qquad\forall\,q^{\mathrm{P}}\in\mathrm{Q}^{\mathrm{P}},
\tag{2.19}
$$

where the vector $\vec{\boldsymbol{\theta}}:=(\boldsymbol{\theta}^{\mathrm{P}},\psi^{\mathrm{P}},\boldsymbol{\theta}^{\mathrm{E}},q^{\mathrm{E}})$, and the boundary and interface conditions suggest defining the involved functional spaces as

$$
\mathbf{H}:=\mathbf{L}^2(\Omega^{\mathrm{P}})\times\mathrm{L}^2(\Omega^{\mathrm{P}})\times\mathbf{L}^2(\Omega^{\mathrm{E}})\times\mathrm{L}^2(\Omega^{\mathrm{E}}),\quad\mathbf{V}:=\mathbf{H}^1_0(\Omega),\quad\mathrm{Q}^{\mathrm{P}}:=\mathrm{H}^1(\Omega^{\mathrm{P}}),
$$

and the bilinear forms $a:\mathbf{H}\times\mathbf{H}\to\mathbb{R}$, $b_1:\mathbf{H}\times\mathbf{V}\to\mathbb{R}$, $b_2:\mathbf{H}\times\mathrm{Q}^{\mathrm{P}}\to\mathbb{R}$, $b_3:\mathbf{H}\times\mathrm{Q}^{\mathrm{P}}\to\mathbb{R}$, $c:\mathrm{Q}^{\mathrm{P}}\times\mathrm{Q}^{\mathrm{P}}\to\mathbb{R}$, and linear functionals $F:\mathbf{V}\to\mathbb{R}$, $G:\mathrm{Q}^{\mathrm{P}}\to\mathbb{R}$

are specified in the following way:

$$a(\vec{\boldsymbol{\omega}},\vec{\boldsymbol{\theta}}) := \int_{\Omega^{\mathrm{P}}} \boldsymbol{\omega}^{\mathrm{P}}\cdot\boldsymbol{\theta}^{\mathrm{P}} + \frac{1}{1+\eta^{\mathrm{P}}}\int_{\Omega^{\mathrm{P}}}\phi^{\mathrm{P}}\psi^{\mathrm{P}} + \int_{\Omega^{\mathrm{E}}}\boldsymbol{\omega}^{\mathrm{E}}\cdot\boldsymbol{\theta}^{\mathrm{E}} + \int_{\Omega^{\mathrm{E}}} p^{\mathrm{E}}q^{\mathrm{E}},$$

$$b_1(\vec{\boldsymbol{\theta}},\boldsymbol{v}) := -\sqrt{\eta^{\mathrm{P}}}\int_{\Omega^{\mathrm{P}}}\boldsymbol{\theta}^{\mathrm{P}}\cdot\mathbf{curl}\,\boldsymbol{v} + \int_{\Omega^{\mathrm{P}}}\psi^{\mathrm{P}}\,\mathrm{div}\,\boldsymbol{v} - \sqrt{\eta^{\mathrm{E}}}\int_{\Omega^{\mathrm{E}}}\boldsymbol{\theta}^{\mathrm{E}}\cdot\mathbf{curl}\,\boldsymbol{v} + \int_{\Omega^{\mathrm{E}}} q^{\mathrm{E}}\,\mathrm{div}\,\boldsymbol{v},$$

$$b_2(\vec{\boldsymbol{\theta}},p^{\mathrm{P}}) := \frac{\alpha}{(1+\eta^{\mathrm{P}})(\lambda^{\mathrm{P}}+\mu^{\mathrm{P}})}\int_{\Omega^{\mathrm{P}}} p^{\mathrm{P}}\psi^{\mathrm{P}}, \qquad b_3(\vec{\boldsymbol{\omega}},q^{\mathrm{P}}) := \frac{\alpha}{(1+\eta^{\mathrm{P}})}\int_{\Omega^{\mathrm{P}}} q^{\mathrm{P}}\phi^{\mathrm{P}},$$

$$c(p^{\mathrm{P}},q^{\mathrm{P}}) := \left[c_0 + \frac{\alpha^2}{(\mu^{\mathrm{P}}+\lambda^{\mathrm{P}})(1+\eta^{\mathrm{P}})}\right]\int_{\Omega^{\mathrm{P}}} p^{\mathrm{P}}q^{\mathrm{P}} + \frac{1}{\xi}\int_{\Omega^{\mathrm{P}}}\kappa\nabla p^{\mathrm{P}}\cdot\nabla q^{\mathrm{P}},$$

$$F(\boldsymbol{v}) := -\int_{\Omega^{\mathrm{P}}}\boldsymbol{f}^{\mathrm{P}}\cdot\boldsymbol{v} - \int_{\Omega^{\mathrm{E}}}\boldsymbol{f}^{\mathrm{E}}\cdot\boldsymbol{v}, \qquad G(q^{\mathrm{P}}) := -\frac{\rho}{\xi}\int_{\Omega^{\mathrm{P}}}\kappa\boldsymbol{g}\cdot\nabla q^{\mathrm{P}} - \int_{\Omega^{\mathrm{P}}} s^{\mathrm{P}}q^{\mathrm{P}}.$$

For the forthcoming analysis, we will consider the following η^{P}- and η^{E}-dependent norms (see, for instance, [24, Remark 2.7]) for the displacements on the solid and elastic domains Ω^{P} and Ω^{E}, respectively:

$$\|\boldsymbol{v}\|^2_{\mathbf{V}^{\mathrm{P}}} := \eta^{\mathrm{P}}\|\mathbf{curl}\,\boldsymbol{v}\|^2_{0,\Omega^{\mathrm{P}}} + \|\mathrm{div}\,\boldsymbol{v}\|^2_{0,\Omega^{\mathrm{P}}} \quad\text{and}\quad \|\boldsymbol{v}\|^2_{\mathbf{V}^{\mathrm{E}}} := \eta^{\mathrm{E}}\|\mathbf{curl}\,\boldsymbol{v}\|^2_{0,\Omega^{\mathrm{E}}} + \|\mathrm{div}\,\boldsymbol{v}\|^2_{0,\Omega^{\mathrm{E}}},$$

which in turn give rise to the following η^{P}- and η^{E}-dependent norm on the space $\mathbf{V}$:

$$\|\boldsymbol{v}\|^2_{\mathbf{V}} := \|\boldsymbol{v}\|^2_{\mathbf{V}^{\mathrm{P}}} + \|\boldsymbol{v}\|^2_{\mathbf{V}^{\mathrm{E}}}.$$

Moreover, $\mathbf{H}$ will be endowed with the norm

$$\|\vec{\boldsymbol{\theta}}\|^2_{\mathbf{H}} := \|\boldsymbol{\theta}^{\mathrm{P}}\|^2_{0,\Omega^{\mathrm{P}}} + \|\psi^{\mathrm{P}}\|^2_{0,\Omega^{\mathrm{P}}} + \|\boldsymbol{\theta}^{\mathrm{E}}\|^2_{0,\Omega^{\mathrm{E}}} + \|q^{\mathrm{E}}\|^2_{0,\Omega^{\mathrm{E}}}.$$

Remark 2.2. We observe that the natural regularity for variable $\boldsymbol{u}$ (and test function $\boldsymbol{v}$) in system (2.17)–(2.19) is $H_0(\mathbf{curl},\Omega)\cap H_0(\mathrm{div},\Omega)$. However, according to [24, Lemma 2.5], an algebraic and topological equivalence between this space and $\mathbf{V}$ holds if the domain Ω is a polyhedral bounded domain with Lipschitz boundary $\partial\Omega$ (see also [24, Remark 2.7]). This permits us, in this particular case, to consider standard finite element subspaces, such as piecewise and continuous polynomials to discretize $\mathbf{V}$. This is the approach we follow in (4.1).

3. Well-posedness analysis. Before addressing the well-posedness of the continuous formulation, we indicate that the bilinear forms and the linear functionals appearing in the variational problem of interest are all bounded by constants independent of η^{P} and η^{E} (see, for instance, [4]). We also recall the positivity of the bilinear forms $a(\cdot,\cdot)$, and $c(\cdot,\cdot)$,

$$a(\vec{\boldsymbol{\theta}},\vec{\boldsymbol{\theta}}) \geq \frac{1}{(1+\eta^{\mathrm{P}})}\|\vec{\boldsymbol{\theta}}\|^2_{\mathbf{H}} \qquad \forall\,\vec{\boldsymbol{\theta}}\in\mathbf{H},$$

$$c(q^{\mathrm{P}},q^{\mathrm{P}}) \geq \left[c_0 + \frac{\alpha^2}{(\mu^{\mathrm{P}}+\lambda^{\mathrm{P}})(1+\eta^{\mathrm{P}})}\right]\|q^{\mathrm{P}}\|_{0,\Omega^{\mathrm{P}}} + \frac{\kappa_1}{\xi}|q^{\mathrm{P}}|_{1,\Omega^{\mathrm{P}}} \qquad \forall\,q^{\mathrm{P}}\in\mathrm{Q}^{\mathrm{P}},$$

as well as the continuous inf-sup condition satisfied by $b_1(\cdot,\cdot)$, stated in the following result.

LEMMA 3.1. *There exists $\beta>0$, independent of η^{P} and η^{E}, such that*

$$\sup_{\vec{\boldsymbol{\theta}}\in\mathbf{H}\setminus\mathbf{0}}\frac{b_1(\vec{\boldsymbol{\theta}},\boldsymbol{v})}{\|\vec{\boldsymbol{\theta}}\|_{\mathbf{H}}} \geq \beta\|\boldsymbol{v}\|_{\mathbf{V}} \qquad \forall\,\boldsymbol{v}\in\mathbf{V}. \tag{3.1}$$

Proof. Proceeding as in [4, Lemma 2.2], let us consider an arbitrary $\boldsymbol{v} \in \mathbf{V}$ and define

$$\vec{\boldsymbol{\theta}}_\beta := (-\sqrt{\eta^{\mathrm{P}}}\,\mathbf{curl}\,\boldsymbol{v}|_{\Omega^{\mathrm{P}}}, \mathrm{div}(\boldsymbol{v})|_{\Omega^{\mathrm{P}}}, -\sqrt{\eta^{\mathrm{E}}}\,\mathbf{curl}\,\boldsymbol{v}|_{\Omega^{\mathrm{E}}}, \mathrm{div}(\boldsymbol{v})|_{\Omega^{\mathrm{E}}}) \in \mathbf{H}.$$

In this way, noting that

$$\|\vec{\boldsymbol{\theta}}_\beta\|_{\mathbf{H}} \leq \|\boldsymbol{v}\|_{\mathbf{V}},$$

and using the definition of $b_1(\cdot,\cdot)$, we readily obtain

$$\sup_{\vec{\boldsymbol{\theta}} \in \mathbf{H}\setminus\mathbf{0}} \frac{b_1(\vec{\boldsymbol{\theta}}, \boldsymbol{v})}{\|\vec{\boldsymbol{\theta}}\|_{\mathbf{H}}} \geq \frac{b_1(\vec{\boldsymbol{\theta}}_\beta, \boldsymbol{v})}{\|\vec{\boldsymbol{\theta}}_\beta\|_{\mathbf{H}}} \geq \beta\|\boldsymbol{v}\|_{\mathbf{V}} \qquad \forall\, \boldsymbol{v} \in \mathbf{H},$$

where we highlight that the constant β is strictly positive and independent of the auxiliary scaling parameters η^{P} and η^{E}. ∎

3.1. Stability. In this section we establish the stability of the problem by combining the boundedness, positivity, and inf-sup conditions from section 2. We begin with the following result.

LEMMA 3.2. *Let* $(\vec{\boldsymbol{\omega}}, \boldsymbol{u}, p^{\mathrm{P}}) \in \mathbf{H} \times \mathbf{V} \times \mathrm{Q}^{\mathrm{P}}$ *be a solution of the system* (2.17)–(2.19)*; then there exists a constant* $C > 0$*, independent of* η^{P} *and* η^{E}*, such that*

(3.2)
$$\|\vec{\boldsymbol{\omega}}\|_{\mathbf{H}} + \|\boldsymbol{u}\|_{\mathbf{V}} + \|p^{\mathrm{P}}\|_{1,\Omega^{\mathrm{P}}} \leq C\big\{(\mu^{\mathrm{P}}+\lambda^{\mathrm{P}})(\|\boldsymbol{f}^{\mathrm{E}}\|_{0,\Omega^{\mathrm{E}}} + \|\boldsymbol{f}^{\mathrm{P}}\|_{0,\Omega^{\mathrm{P}}}) + \|\boldsymbol{g}\|_{0,\Omega^{\mathrm{P}}} + \|s^{\mathrm{P}}\|_{0,\Omega^{\mathrm{P}}}\big\}.$$

Proof. We start by considering $\vec{\boldsymbol{\theta}} = \vec{\boldsymbol{\omega}}$ in (2.17) and $\boldsymbol{v} = \boldsymbol{u}$ in (2.18). Thus, combining both equations and applying the ellipticity of the bilinear form $a(\cdot,\cdot)$, we obtain

$$\begin{aligned}\frac{1}{1+\eta^{\mathrm{P}}}\|\vec{\boldsymbol{\omega}}\|^2_{\mathbf{H}} \leq a(\vec{\boldsymbol{\omega}}, \vec{\boldsymbol{\omega}}) &\leq \frac{\alpha}{(1+\eta^{\mathrm{P}})(\mu^{\mathrm{P}}+\lambda^{\mathrm{P}})}\|\vec{\boldsymbol{\omega}}\|_{\mathbf{H}}\|p^{\mathrm{P}}\|_{0,\Omega^{\mathrm{P}}} \\ &\quad + (\|\boldsymbol{f}^{\mathrm{P}}\|_{0,\Omega^{\mathrm{P}}} + \|\boldsymbol{f}^{\mathrm{E}}\|_{0,\Omega^{\mathrm{E}}})\|\boldsymbol{u}\|_{0,\Omega}\end{aligned}$$

which, by using the classical Young's inequality, can be rewritten as

(3.3)
$$\frac{1}{2(1+\eta^{\mathrm{P}})}\|\vec{\boldsymbol{\omega}}\|^2_{\mathbf{H}} \leq \frac{\alpha^2}{2(1+\eta^{\mathrm{P}})(\mu^{\mathrm{P}}+\lambda^{\mathrm{P}})^2}\|p^{\mathrm{P}}\|^2_{0,\Omega^{\mathrm{P}}} + (\|\boldsymbol{f}^{\mathrm{P}}\|_{0,\Omega^{\mathrm{P}}} + \|\boldsymbol{f}^{\mathrm{E}}\|_{0,\Omega^{\mathrm{E}}})\|\boldsymbol{u}\|_{0,\Omega}$$

or, equivalently,

$$\begin{aligned}\frac{(\mu^{\mathrm{P}}+\lambda^{\mathrm{P}})}{2(1+\eta^{\mathrm{P}})}\|\vec{\boldsymbol{\omega}}\|^2_{\mathbf{H}} &\leq \frac{\alpha^2}{2(1+\eta^{\mathrm{P}})(\mu^{\mathrm{P}}+\lambda^{\mathrm{P}})}\|p^{\mathrm{P}}\|^2_{0,\Omega^{\mathrm{P}}} \\ &\quad + (\mu^{\mathrm{P}}+\lambda^{\mathrm{P}})(\|\boldsymbol{f}^{\mathrm{P}}\|_{0,\Omega^{\mathrm{P}}} + \|\boldsymbol{f}^{\mathrm{E}}\|_{0,\Omega^{\mathrm{E}}})\|\boldsymbol{u}\|_{0,\Omega}.\end{aligned} \tag{3.4}$$

Furthermore, choosing $q^{\mathrm{P}} = p^{\mathrm{P}}$ in (2.19) and applying the positivity of $c(\cdot,\cdot)$, we get

$$\begin{aligned}&\left[c_0 + \frac{\alpha^2}{(\mu^{\mathrm{P}}+\lambda^{\mathrm{P}})(1+\eta^{\mathrm{P}})}\right]\|p^{\mathrm{P}}\|^2_{0,\Omega^{\mathrm{P}}} + \frac{\kappa_1}{\xi}|p^{\mathrm{P}}|^2_{1,\Omega^{\mathrm{P}}} \\ &\qquad \leq \frac{\alpha}{1+\eta^{\mathrm{P}}}\|\vec{\boldsymbol{\omega}}\|_{\mathbf{H}}\|p^{\mathrm{P}}\|_{0,\Omega^{\mathrm{P}}} + (\rho\xi^{-1}\kappa_2\|\boldsymbol{g}\|_{0,\Omega^{\mathrm{P}}} + \|s^{\mathrm{P}}\|_{0,\Omega^{\mathrm{P}}})\|p^{\mathrm{P}}\|_{1,\Omega^{\mathrm{P}}},\end{aligned} \tag{3.5}$$

such that applying Young's inequality with constant $\delta := \frac{\mu^{\mathrm{P}}+\lambda^{\mathrm{P}}}{\alpha}$ to the first term on the right-hand side of (3.5) and then using (3.4) gives

$$\begin{aligned}\left[c_0 + \frac{\alpha^2}{(\mu^{\mathrm{P}}+\lambda^{\mathrm{P}})(1+\eta^{\mathrm{P}})}\right]\|p^{\mathrm{P}}\|^2_{0,\Omega^{\mathrm{P}}} + \frac{\kappa_1}{\xi}|p^{\mathrm{P}}|^2_{1,\Omega^{\mathrm{P}}} &\leq \frac{\alpha^2}{(\mu^{\mathrm{P}}+\lambda^{\mathrm{P}})(1+\eta^{\mathrm{P}})}\|p^{\mathrm{P}}\|^2_{0,\Omega^{\mathrm{P}}} \\ &+ (\mu^{\mathrm{P}}+\lambda^{\mathrm{P}})(\|\boldsymbol{f}^{\mathrm{P}}\|_{0,\Omega^{\mathrm{P}}} + \|\boldsymbol{f}^{\mathrm{E}}\|_{0,\Omega^{\mathrm{E}}})\|\boldsymbol{u}\|_{0,\Omega} \\ &+ (\rho\xi^{-1}\kappa_2\|\boldsymbol{g}\|_{0,\Omega^{\mathrm{P}}} + \|s^{\mathrm{P}}\|_{0,\Omega^{\mathrm{P}}})\|p^{\mathrm{P}}\|_{1,\Omega^{\mathrm{P}}}\end{aligned}$$

or, equivalently,

$$\begin{aligned}c_1\|p^{\mathrm{P}}\|^2_{1,\Omega^{\mathrm{P}}} &\leq (\mu^{\mathrm{P}}+\lambda^{\mathrm{P}})(\|\boldsymbol{f}^{\mathrm{P}}\|_{0,\Omega^{\mathrm{P}}} + \|\boldsymbol{f}^{\mathrm{E}}\|_{0,\Omega^{\mathrm{E}}})\|\boldsymbol{u}\|_{0,\Omega} \\ &+ (\rho\xi^{-1}\kappa_2\|\boldsymbol{g}\|_{0,\Omega^{\mathrm{P}}} + \|s^{\mathrm{P}}\|_{0,\Omega^{\mathrm{P}}})\|p^{\mathrm{P}}\|_{1,\Omega^{\mathrm{P}}},\end{aligned} \tag{3.6}$$

where $c_1 := \min\{c_0, \kappa_1\xi^{-1}\}$. On the other hand, by combining (3.3) and (3.5), we obtain

$$\begin{aligned}\frac{1}{1+\eta^{\mathrm{P}}}\|\vec{\boldsymbol{\omega}}\|^2_{\mathbf{H}} &\leq \frac{\alpha}{1+\eta^{\mathrm{P}}}\|\vec{\boldsymbol{\omega}}\|_{\mathbf{H}}\|p^{\mathrm{P}}\|_{0,\Omega^{\mathrm{P}}} \\ &+ 2(\|\boldsymbol{f}^{\mathrm{P}}\|_{0,\Omega^{\mathrm{P}}} + \|\boldsymbol{f}^{\mathrm{E}}\|_{0,\Omega^{\mathrm{E}}})\|\boldsymbol{u}\|_{0,\Omega} + (\rho\xi^{-1}\kappa_2\|\boldsymbol{g}\|_{0,\Omega^{\mathrm{P}}} + \|s^{\mathrm{P}}\|_{0,\Omega^{\mathrm{P}}})\|p^{\mathrm{P}}\|_{1,\Omega^{\mathrm{P}}},\end{aligned}$$

which, applying Young's inequality, leads to

$$\begin{aligned}\frac{1}{2(1+\eta^{\mathrm{P}})}\|\vec{\boldsymbol{\omega}}\|^2_{\mathbf{H}} &\leq \frac{\alpha^2}{2(1+\eta^{\mathrm{P}})}\|p^{\mathrm{P}}\|^2_{0,\Omega^{\mathrm{P}}} \\ &+ 2(\|\boldsymbol{f}^{\mathrm{P}}\|_{0,\Omega^{\mathrm{P}}} + \|\boldsymbol{f}^{\mathrm{E}}\|_{0,\Omega^{\mathrm{E}}})\|\boldsymbol{u}\|_{0,\Omega} + (\rho\xi^{-1}\kappa_2\|\boldsymbol{g}\|_{0,\Omega^{\mathrm{P}}} + \|s^{\mathrm{P}}\|_{0,\Omega^{\mathrm{P}}})\|p^{\mathrm{P}}\|_{1,\Omega^{\mathrm{P}}}.\end{aligned} \tag{3.7}$$

Now, from the inf-sup condition (3.1) with $\boldsymbol{v} = \boldsymbol{u}$ and using (2.17), we get

$$\beta\|\boldsymbol{u}\|_{\mathbf{V}} \leq \frac{\alpha}{(\mu^{\mathrm{P}}+\lambda^{\mathrm{P}})(1+\eta^{\mathrm{P}})}\|p^{\mathrm{P}}\|_{0,\Omega^{\mathrm{P}}} + \|\vec{\boldsymbol{\omega}}\|_{\mathbf{H}}. \tag{3.8}$$

Finally, substituting (3.8) back into (3.6) and (3.7), and then applying Young's inequality whenever adequate, we obtain the desired result. ∎

Remark 3.1. The expression $(\mu^{\mathrm{P}}+\lambda^{\mathrm{P}})(\|\boldsymbol{f}^{\mathrm{E}}\|_{0,\Omega^{\mathrm{E}}} + \|\boldsymbol{f}^{\mathrm{P}}\|_{0,\Omega^{\mathrm{P}}})$ in (3.2) must be understood as a term independent of λ^{P} since, from the definitions introduced in section 2 for $\boldsymbol{f}^{\mathrm{P}}$ and $\boldsymbol{f}^{\mathrm{E}}$, together with Remark 2.1, and assuming that $(\mu^{\mathrm{P}}+\lambda^{\mathrm{P}}) \sim (\mu^{\mathrm{E}}+\lambda^{\mathrm{E}})$, we deduce that $(\mu^{\mathrm{P}}+\lambda^{\mathrm{P}})(\|\boldsymbol{f}^{\mathrm{P}}\|_{0,\Omega^{\mathrm{P}}} + \|\boldsymbol{f}^{\mathrm{E}}\|_{0,\Omega^{\mathrm{E}}}) \sim (\|\widetilde{\boldsymbol{f}}^{\mathrm{P}}\|_{0,\Omega^{\mathrm{P}}} + \|\widetilde{\boldsymbol{f}}^{\mathrm{E}}\|_{0,\Omega^{\mathrm{E}}})$.

Remark 3.2. In the case when $c_0 \to 0$ in (2.2), the problem for the fluid pressure p^{P} defined in (2.1)–(2.2) is not well-posed in $\mathrm{H}^1(\Omega^{\mathrm{P}})$. However, uniqueness is restored by asking the solution to live in $\mathrm{H}^1(\Omega^{\mathrm{P}}) \cap \mathrm{L}^2_0(\Omega^{\mathrm{P}})$, where $\mathrm{L}^2_0(\Omega^{\mathrm{P}}) := \{q \in \mathrm{L}^2(\Omega^{\mathrm{P}}) : \int_{\Omega^{\mathrm{P}}} q = 0\}$. As this new space is a closed subspace of $\mathrm{H}^1(\Omega^{\mathrm{P}})$, where the norm and seminorm are equivalent, the stability analysis of (2.17)–(2.19) follows exactly as in Lemma 3.2, with the constant c_1 in (3.6) now defined as $c_1 := c_p\kappa_1\xi^{-1}$, with c_p representing the Poincaré constant.

3.2. Solvability of the continuous problem. We now address the unique solvability of (2.17)–(2.19), applying Fredholm's alternative theory for compact operators. Let us recast the system (2.17)–(2.19) as the following equivalent operator problem: find $\vec{\boldsymbol{u}} := (\vec{\boldsymbol{\omega}}, \boldsymbol{u}, p^{\mathrm{P}}) \in \mathbf{X} := \mathbf{H} \times \mathbf{V} \times \mathrm{Q}^{\mathrm{P}}$ such that

$$(\mathcal{S}+\mathcal{T})\vec{\boldsymbol{u}} = \mathcal{F}, \tag{3.9}$$

where the linear operators $\mathcal{S} : \mathbf{X} \to \mathbf{X}^\star$, $\mathcal{T} : \mathbf{X} \to \mathbf{X}^\star$, and $\mathcal{F} \in \mathbf{X}^\star$ are defined as

$$\begin{aligned}\langle \mathcal{S}(\vec{\boldsymbol{u}}), \vec{\boldsymbol{v}} \rangle &:= a(\vec{\boldsymbol{\omega}}, \vec{\boldsymbol{\theta}}) + b_1(\vec{\boldsymbol{\theta}}, \boldsymbol{u}) - b_1(\vec{\boldsymbol{\omega}}, \boldsymbol{v}) + c(p^{\mathrm{P}}, q^{\mathrm{P}}),\\ \langle \mathcal{T}(\vec{\boldsymbol{u}}), \vec{\boldsymbol{v}} \rangle &:= -b_2(\vec{\boldsymbol{\theta}}, p^{\mathrm{P}}) - b_3(\vec{\boldsymbol{\omega}}, q^{\mathrm{P}}),\\ \langle \mathcal{F}, \vec{\boldsymbol{v}} \rangle &:= -F(\boldsymbol{v}) - G(q^{\mathrm{P}})\end{aligned}$$

for all $\vec{\boldsymbol{u}} := (\vec{\boldsymbol{\omega}}, \boldsymbol{u}, p^{\mathrm{P}})$, $\vec{\boldsymbol{v}} := (\vec{\boldsymbol{\theta}}, \boldsymbol{v}, q^{\mathrm{P}}) \in \mathbf{X}$, where we recall that $\langle \cdot, \cdot \rangle$ stands for the duality pairing between the space $\mathbf{X}$ and its dual $\mathbf{X}^\star$.

The three upcoming lemmas establish the invertibility of $\mathcal{S}$, the compactness of $\mathcal{T}$, and the injectivity of $\mathcal{S}+\mathcal{T}$, such that Fredholm's theory implies the well-posedness of the operator problem (3.9) and, equivalently, of (2.17)–(2.19).

LEMMA 3.3. *The operator $\mathcal{S} : \mathbf{X} \to \mathbf{X}^\star$ is invertible.*

Proof. First, for a given functional $\mathcal{F} := (\mathcal{F}_{\mathbf{H}}, \mathcal{F}_{\mathbf{V}}, \mathcal{F}_{\mathrm{Q}^{\mathrm{P}}})$, observe that establishing the invertibility of $\mathcal{S}$ is equivalent to proving the unique solvability of the operator problem

$$\mathcal{S}(\vec{\boldsymbol{u}}) = \mathcal{F}. \tag{3.10}$$

Furthermore, proving unique solvability of (3.10) is in turn equivalent to proving the unique solvability of the two following uncoupled problems: find $(\vec{\boldsymbol{\omega}}, \boldsymbol{u}) \in \mathbf{H} \times \mathbf{V}$ such that

$$\begin{aligned} a(\vec{\boldsymbol{\omega}}, \vec{\boldsymbol{\theta}}) + b_1(\vec{\boldsymbol{\theta}}, \boldsymbol{u}) &= F_{\mathbf{H}}(\vec{\boldsymbol{\theta}}) \qquad \forall\, \vec{\boldsymbol{\theta}} \in \mathbf{H},\\ b_1(\vec{\boldsymbol{\omega}}, \boldsymbol{v}) &= F_{\mathbf{V}}(\boldsymbol{v}) \qquad \forall\, \boldsymbol{v} \in \mathbf{V},\end{aligned} \tag{3.11}$$

and find $p^{\mathrm{P}} \in \mathrm{Q}^{\mathrm{P}}$ such that

$$c(p^{\mathrm{P}}, q^{\mathrm{P}}) = F_{\mathrm{Q}^{\mathrm{P}}}(q^{\mathrm{P}}) \qquad \forall q^{\mathrm{P}} \in \mathrm{Q}^{\mathrm{P}}, \tag{3.12}$$

where $F_{\mathbf{H}}$, $F_{\mathbf{V}}$, and $F_{\mathrm{Q}^{\mathrm{P}}}$ are the functionals induced by $\mathcal{F}_{\mathbf{H}}$, $\mathcal{F}_{\mathbf{V}}$, and $\mathcal{F}_{\mathrm{Q}^{\mathrm{P}}}$, respectively.

Observe that the unique solvability of the latter problem (3.12) follows by virtue of the well-known Lax–Milgram lemma. In turn, according to the continuity of $a(\cdot, \cdot)$, and $b_1(\cdot, \cdot)$, the ellipticity of $a(\cdot, \cdot)$ and the inf-sup condition of $b_1(\cdot, \cdot)$, the well-posedness of (3.11) follows from a straightforward application of the Babuška–Brezzi theory (see, e.g., [20, Theorem 2.3]), completing the proof. ∎

LEMMA 3.4. *The operator $\mathcal{T} : \mathbf{X} \to \mathbf{X}^\star$ is compact.*

Proof. We begin by defining the operator $\mathbb{B} : \mathrm{L}^2(\Omega^{\mathrm{P}}) \to \mathrm{Q}^{\mathrm{P}}$ as

$$\langle \mathbb{B}(\psi^{\mathrm{P}}), q^{\mathrm{P}} \rangle_{0,\Omega^{\mathrm{P}}} := \alpha(1 + \eta^{\mathrm{P}})^{-1} \int_{\Omega^{\mathrm{P}}} q^{\mathrm{P}} \psi^{\mathrm{P}} \quad \forall\, q^{\mathrm{P}} \in \mathrm{Q}^{\mathrm{P}}, \quad \forall\, \psi^{\mathrm{P}} \in \mathrm{L}^2(\Omega^{\mathrm{P}}),$$

where $\langle \cdot, \cdot \rangle_{0,\Omega^{\mathrm{P}}}$ denotes the $\mathrm{L}^2(\Omega^{\mathrm{P}})$-inner product. This operator is compact since it consists of the composition of a compact injection and a continuous map (see [38, Lemma 2.2] for further details). Thus, denoting by $\mathbb{B}^\star$ the adjoint of $\mathbb{B}$, we infer that the operator

$$\mathcal{T}(\vec{\boldsymbol{u}}) = ((\mathbf{0}, -(\mu^{\mathrm{P}} + \lambda^{\mathrm{P}})^{-1} \mathbb{B}(\phi^{\mathrm{P}}), \mathbf{0}, 0), \mathbf{0}, -\mathbb{B}^\star(p^{\mathrm{P}}))$$

is also compact. ∎

LEMMA 3.5. *The operator* $(\mathcal{S}+\mathcal{T}) : \mathbf{X} \to \mathbf{X}^\star$ *is injective.*

Proof. By definition of the linear operator $(\mathcal{S}+\mathcal{T}) : \mathbf{X} \to \mathbf{X}^\star$, observe that it is sufficient to show that the only solution to the homogeneous problem

$$\begin{aligned} a(\vec{\boldsymbol{\omega}}, \vec{\boldsymbol{\theta}}) + b_1(\vec{\boldsymbol{\theta}}, \boldsymbol{u}) - b_2(\vec{\boldsymbol{\theta}}, p^{\mathrm{P}}) &= 0 \qquad \forall\, \vec{\boldsymbol{\theta}} \in \mathbf{H}, \\ b_1(\vec{\boldsymbol{\omega}}, \boldsymbol{v}) &= 0 \qquad \forall\, \boldsymbol{v} \in \mathbf{V}, \\ b_3(\vec{\boldsymbol{\omega}}, q^{\mathrm{P}}) - c(p^{\mathrm{P}}, q^{\mathrm{P}}) &= 0 \qquad \forall\, q^{\mathrm{P}} \in \mathrm{Q}^{\mathrm{P}} \end{aligned}$$

is the null-vector in the product space $\mathbf{X}$. Thus, from (3.6), (3.7), and the fact that $F = G = 0$, we deduce that $\vec{\boldsymbol{\omega}} = \mathbf{0}$ and $p = 0$. Then, with this in mind, we apply (3.8) and obtain $\boldsymbol{u} = \mathbf{0}$, which finishes the proof. ∎

By virtue of Lemmas 3.2–3.5 and the abstract Fredholm alternative theorem, one straightforwardly derives the main result of this section, stated in the following theorem.

THEOREM 3.1. *There exists a unique solution* $(\vec{\boldsymbol{\omega}}, \boldsymbol{u}, p^{\mathrm{P}}) \in \mathbf{H} \times \mathbf{V} \times \mathrm{Q}^{\mathrm{P}}$ *to the coupled problem* (2.17)–(2.19). *Furthermore, there exists a positive constant* $C > 0$, *independent of* η^{P} *and* η^{E}, *such that*

$$\begin{aligned} &\|\vec{\boldsymbol{\omega}}\|_{\mathbf{H}} + \|\boldsymbol{u}\|_{\mathbf{V}} + \|p^{\mathrm{P}}\|_{1,\Omega^{\mathrm{P}}} \\ &\leq C\big\{(\mu^{\mathrm{P}} + \lambda^{\mathrm{P}})(\|\boldsymbol{f}^{\mathrm{E}}\|_{0,\Omega^{\mathrm{E}}} + \|\boldsymbol{f}^{\mathrm{P}}\|_{0,\Omega^{\mathrm{P}}}) + \|\boldsymbol{g}\|_{0,\Omega^{\mathrm{P}}} + \|s^{\mathrm{P}}\|_{0,\Omega^{\mathrm{P}}}\big\}. \end{aligned}$$

4. Finite element discretization.

4.1. Discrete spaces and Galerkin formulation. Let $\{\mathcal{T}_h\}_{h>0}$ be a shape-regular family of partitions of the closed domain $\bar{\Omega}$, conformed by tetrahedra (or triangles in 2D) T of diameter h_T, with mesh size $h := \max\{h_T : T \in \mathcal{T}_h\}$. Given an integer $k \geq 0$ and a subset S of $\mathbb{R}^d$, $d = 2, 3$, by $\mathbb{P}_k(S)$ we will denote the space of polynomial functions defined locally in S and being of total degree up to k.

We specify the finite-dimensional subspaces of the functional spaces for global displacement, fluid poroelastic pressure, poroelastic rotations, total poroelastic pressure, elastic rotations, and solid pressure as follows:

$$\begin{aligned} \mathbf{V}_h &:= \{\boldsymbol{v}_h \in \mathbf{C}(\bar{\Omega}) \cap \mathbf{V} : \boldsymbol{v}_h|_T \in \mathbb{P}_{k+1}(T)^d \ \forall T \in \mathcal{T}_h\}, \\ \mathrm{Q}_h^{\mathrm{P}} &:= \{q_h^{\mathrm{P}} \in \mathrm{C}(\overline{\Omega^{\mathrm{P}}}) : q_h^{\mathrm{P}}|_T \in \mathbb{P}_{k+1}(T) \ \forall T \in \mathcal{T}_h\}, \\ \mathbf{W}_h^{\mathrm{P}} &:= \{\boldsymbol{\theta}_h^{\mathrm{P}} \in \mathbf{L}^2(\Omega^{\mathrm{P}}) : \boldsymbol{\theta}_h^{\mathrm{P}}|_T \in \mathbb{P}_k(T)^d \ \forall T \in \mathcal{T}_h\}, \\ \mathrm{Z}_h^{\mathrm{P}} &:= \{\psi_h^{\mathrm{P}} \in \mathrm{L}^2(\Omega^{\mathrm{P}}) : \psi_h^{\mathrm{P}}|_T \in \mathbb{P}_k(T) \ \forall T \in \mathcal{T}_h\}, \\ \mathbf{W}_h^{\mathrm{E}} &:= \{\boldsymbol{\theta}_h^{\mathrm{E}} \in \mathbf{L}^2(\Omega^{\mathrm{E}}) : \boldsymbol{\theta}_h^{\mathrm{E}}|_T \in \mathbb{P}_k(T)^d \ \forall T \in \mathcal{T}_h\}, \\ \mathrm{Q}_h^{\mathrm{E}} &:= \{q_h^{\mathrm{E}} \in \mathrm{L}^2(\Omega^{\mathrm{E}}) : q_h^{\mathrm{E}}|_T \in \mathbb{P}_k(T), \ \forall T \in \mathcal{T}_h\}. \end{aligned} \tag{4.1}$$

In this way, denoting by $\vec{\boldsymbol{\omega}}_h := (\boldsymbol{\omega}_h^{\mathrm{P}}, \phi_h^{\mathrm{P}}, \boldsymbol{\omega}_h^{\mathrm{E}}, p_h^{\mathrm{E}}) \in \mathbf{W}_h^{\mathrm{P}} \times \mathrm{Z}_h^{\mathrm{P}} \times \mathbf{W}_h^{\mathrm{E}} \times \mathrm{Q}_h^{\mathrm{E}} := \mathbf{H}_h$, the proposed Galerkin finite element scheme approximating (2.17)–(2.19) reads as follows: find $(\vec{\boldsymbol{\omega}}_h, \boldsymbol{u}_h, p_h^{\mathrm{P}}) \in \mathbf{H}_h \times \mathbf{V}_h \times \mathrm{Q}_h^{\mathrm{P}}$ such that

$$a(\vec{\boldsymbol{\omega}}_h, \vec{\boldsymbol{\theta}}_h) + b_1(\vec{\boldsymbol{\theta}}_h, \boldsymbol{u}_h) - b_2(\vec{\boldsymbol{\theta}}_h, p_h^{\mathrm{P}}) = 0 \qquad \forall\, \vec{\boldsymbol{\theta}}_h \in \mathbf{H}_h, \tag{4.2}$$

$$b_1(\vec{\boldsymbol{\omega}}_h, \boldsymbol{v}_h) = F(\boldsymbol{v}_h) \qquad \forall\, \boldsymbol{v}_h \in \mathbf{V}_h, \tag{4.3}$$

$$b_3(\vec{\boldsymbol{\omega}}_h, q_h^{\mathrm{P}}) - c(p_h^{\mathrm{P}}, q_h^{\mathrm{P}}) = G(q_h^{\mathrm{P}}) \qquad \forall\, q_h^{\mathrm{P}} \in \mathrm{Q}_h^{\mathrm{P}}, \tag{4.4}$$

where $\vec{\boldsymbol{\theta}}_h := (\boldsymbol{\theta}_h^{\mathrm{P}}, \psi_h^{\mathrm{P}}, \boldsymbol{\theta}_h^{\mathrm{E}}, q_h^{\mathrm{E}})$.

4.2. Solvability and stability of the discrete problem. It is evident that all bilinear forms and functionals introduced in section 2 preserve the relevant stability properties on the corresponding discrete spaces. Furthermore, it is clear that the bilinear forms $a(\cdot,\cdot)$, and $c(\cdot,\cdot)$ also maintain the coercivity on the discrete spaces $\mathbf{H}_h$ and $\mathrm{Q}_h^{\mathrm{P}}$, respectively. Moreover, we notice in advance that the continuous inf-sup condition (3.1) is also inherited at the discrete level for the particular choice of elements outlined in (4.1), and therefore, there exists a positive constant $\widehat{\beta}$ independent of h such that the following holds:

$$\sup_{\vec{\boldsymbol{\theta}}_h \in \mathbf{H}_h \setminus \mathbf{0}} \frac{b_1(\vec{\boldsymbol{\theta}}_h, \boldsymbol{v}_h)}{\|\vec{\boldsymbol{\theta}}_h\|_{\mathbf{H}}} \geq \widehat{\beta} \|\boldsymbol{v}_h\|_{\mathbf{V}} \qquad \forall\, \boldsymbol{v}_h \in \mathbf{V}_h, \tag{4.5}$$

where we once again mention that $\widehat{\beta}$ is independent of the auxiliary scaling parameters η^{P} and η^{E}.

Next, utilizing the stability properties outlined above, we are ready to establish the well-posedness of the proposed Galerkin scheme (4.2)–(4.4).

THEOREM 4.1. *There exists a unique solution* $(\vec{\boldsymbol{\omega}}_h, \boldsymbol{u}_h, p_h^{\mathrm{P}}) \in \mathbf{H}_h \times \mathbf{V}_h \times \mathrm{Q}_h^{\mathrm{P}}$ *to the discrete coupled problem* (4.2)–(4.4). *Furthermore, there exists a positive constant* $C_{Stab} > 0$, *independent of* h, η^{P}, *and* η^{E}, *such that*

$$\begin{aligned} &\|\vec{\boldsymbol{\omega}}_h\|_{\mathbf{H}} + \|\boldsymbol{u}_h\|_{\mathbf{V}} + \|p_h^{\mathrm{P}}\|_{1,\Omega^{\mathrm{P}}} \\ &\leq C_{Stab}\big\{(\mu^{\mathrm{P}} + \lambda^{\mathrm{P}})(\|\boldsymbol{f}^{\mathrm{E}}\|_{0,\Omega^{\mathrm{E}}} + \|\boldsymbol{f}^{\mathrm{P}}\|_{0,\Omega^{\mathrm{P}}}) + \|\boldsymbol{g}\|_{0,\Omega^{\mathrm{P}}} + \|s^{\mathrm{P}}\|_{0,\Omega^{\mathrm{P}}}\big\}. \end{aligned}$$

Proof. First, for the stability analysis, we proceed exactly as in the proof of Lemma 3.2. Thus, it is a laborious but straightforward exercise to verify that

$$\begin{aligned} c_1\|p_h^{\mathrm{P}}\|_{1,\Omega^{\mathrm{P}}}^2 &\leq (\mu^{\mathrm{P}} + \lambda^{\mathrm{P}})(\|\boldsymbol{f}^{\mathrm{P}}\|_{0,\Omega^{\mathrm{P}}} + \|\boldsymbol{f}^{\mathrm{E}}\|_{0,\Omega^{\mathrm{E}}})\|\boldsymbol{u}_h\|_{0,\Omega} \\ &\quad + (\rho\xi^{-1}\kappa_2\|\boldsymbol{g}\|_{0,\Omega^{\mathrm{P}}} + \|s^{\mathrm{P}}\|_{0,\Omega^{\mathrm{P}}})\|p_h^{\mathrm{P}}\|_{1,\Omega^{\mathrm{P}}}, \\ \frac{1}{2(1+\eta^{\mathrm{P}})}\|\vec{\boldsymbol{\omega}}_h\|_{\mathbf{H}}^2 &\leq \frac{\alpha^2}{2(1+\eta^{\mathrm{P}})}\|p_h^{\mathrm{P}}\|_{0,\Omega^{\mathrm{P}}}^2 + 2(\|\boldsymbol{f}^{\mathrm{P}}\|_{0,\Omega^{\mathrm{P}}} + \|\boldsymbol{f}^{\mathrm{E}}\|_{0,\Omega^{\mathrm{E}}})\|\boldsymbol{u}_h\|_{0,\Omega} \\ &\quad + (\rho\xi^{-1}\kappa_2\|\boldsymbol{g}\|_{0,\Omega^{\mathrm{P}}} + \|s^{\mathrm{P}}\|_{0,\Omega^{\mathrm{P}}})\|p_h^{\mathrm{P}}\|_{1,\Omega^{\mathrm{P}}}, \\ \beta\|\boldsymbol{u}_h\|_{\mathbf{V}} &\leq \frac{\alpha}{(\mu^{\mathrm{P}} + \lambda^{\mathrm{P}})(1+\eta^{\mathrm{P}})}\|p_h^{\mathrm{P}}\| + \|\vec{\boldsymbol{\omega}}_h\|_{\mathbf{H}}, \end{aligned}$$

which imply that there exists $C_{\mathrm{Stab}} > 0$, independent of h, η^{P}, and η^{E}, such that

$$\begin{aligned} &\|\vec{\boldsymbol{\omega}}_h\|_{\mathbf{H}} + \|\boldsymbol{u}_h\|_{\mathbf{V}} + \|p_h^{\mathrm{P}}\|_{1,\Omega^{\mathrm{P}}} \\ &\leq C_{\mathrm{Stab}}\big\{(\mu^{\mathrm{P}} + \lambda^{\mathrm{P}})(\|\boldsymbol{f}^{\mathrm{E}}\|_{0,\Omega^{\mathrm{E}}} + \|\boldsymbol{f}^{\mathrm{P}}\|_{0,\Omega^{\mathrm{P}}}) + \|\boldsymbol{g}\|_{0,\Omega^{\mathrm{P}}} + \|s^{\mathrm{P}}\|_{0,\Omega^{\mathrm{P}}}\big\}. \end{aligned} \tag{4.6}$$

For the solvability analysis of the discrete scheme, it suffices to prove that the solution of the homogeneous problem is the trivial solution (since we are restricting to the finite-dimensional case). For this purpose, we let $(\vec{\boldsymbol{\omega}}_h, \boldsymbol{u}_h, p_h^{\mathrm{P}}) \in \mathbf{H}_h \times \mathbf{V}_h \times \mathrm{Q}_h^{\mathrm{P}}$ be the solution to the discrete coupled problem (4.2)–(4.4), where it is assumed that $\boldsymbol{f}^{\mathrm{E}} = \mathbf{0}$, $\boldsymbol{f}^{\mathrm{P}} = \mathbf{0}$, $\boldsymbol{g} = \mathbf{0}$, and $s^{\mathrm{P}} = 0$. Thus, proceeding as in the proof of Lemma 3.5, the result follows straightforwardly by (4.6). ∎

4.3. A priori error bounds. We are now in a position to derive the optimal a priori estimates for the Galerkin scheme (4.2)–(4.4). For this purpose, we first establish a Céa estimate, formulated in the following theorem.

THEOREM 4.2. *Let* $(\vec{\boldsymbol{\omega}}, \boldsymbol{u}, p^{\mathrm{P}})$ *and* $(\vec{\boldsymbol{\omega}}_h, \boldsymbol{u}_h, p_h^{\mathrm{P}})$ *be the unique solutions of the continuous and discrete coupled problems* (2.17)–(2.19) *and* (4.2)–(4.4)*, respectively. Then, there exists a strictly positive constant* $C_{Céa} > 0$*, independent of* h*,* η^{P}*, and* η^{E}*, such that*

$$\begin{aligned}(4.7)\qquad &\|\vec{\boldsymbol{\omega}} - \vec{\boldsymbol{\omega}}_h\|_{\mathbf{H}} + \|\boldsymbol{u} - \boldsymbol{u}_h\|_{\mathbf{V}} + \|p^{\mathrm{P}} - p_h^{\mathrm{P}}\|_{1,\Omega^{\mathrm{P}}} \\ &\leq C_{Céa}\big(\mathrm{dist}(\vec{\boldsymbol{\omega}}, \mathbf{H}_h) + \mathrm{dist}(\boldsymbol{u}, \mathbf{V}_h) + \mathrm{dist}(p^{\mathrm{P}}, \mathrm{Q}_h^{\mathrm{P}})\big).\end{aligned}$$

Proof. First, we start by introducing the discrete space

$$\mathbf{K}_h := \{\vec{\boldsymbol{\theta}}_h \in \mathbf{H}_h : b_1(\vec{\boldsymbol{\theta}}_h, \boldsymbol{v}_h) = F(\boldsymbol{v}_h) \quad \forall \boldsymbol{v}_h \in \mathbf{V}_h\},$$

and observing, according to (4.3), that $\vec{\boldsymbol{\omega}}_h \in \mathbf{K}_h$ and that $(\vec{\boldsymbol{\omega}}_h - \vec{\boldsymbol{\chi}}_{\vec{\boldsymbol{\omega}},h}) \in \mathrm{Ker}_h(b_1) := \{\vec{\boldsymbol{\theta}}_h \in \mathbf{H}_h : b_1(\vec{\boldsymbol{\theta}}_h, \boldsymbol{v}_h) = 0$ for all $\boldsymbol{v}_h \in \mathbf{V}_h\}$ for all $\vec{\boldsymbol{\chi}}_{\vec{\boldsymbol{\omega}},h} \in \mathbf{K}_h$. Moreover, following the arguments employed in [38, Theorem 3.2], we establish the corresponding Galerkin orthogonality property:

$$\begin{aligned}(4.8)\qquad &a(\vec{\boldsymbol{\omega}} - \vec{\boldsymbol{\omega}}_h, \vec{\boldsymbol{\theta}}_h) + b_1(\vec{\boldsymbol{\theta}}_h, \boldsymbol{u} - \boldsymbol{u}_h) - b_2(\vec{\boldsymbol{\theta}}_h, p^{\mathrm{P}} - p_h^{\mathrm{P}}) = 0 \qquad \forall\, \vec{\boldsymbol{\theta}}_h \in \mathbf{H}_h,\\ (4.9)\qquad &b_1(\vec{\boldsymbol{\omega}} - \vec{\boldsymbol{\omega}}_h, \boldsymbol{v}_h) = 0 \qquad \forall\, \boldsymbol{v}_h \in \mathbf{V}_h,\\ (4.10)\qquad &b_3(\vec{\boldsymbol{\omega}} - \vec{\boldsymbol{\omega}}_h, q_h^{\mathrm{P}}) - c(p^{\mathrm{P}} - p_h^{\mathrm{P}}, q_h^{\mathrm{P}}) = 0 \qquad \forall\, q_h^{\mathrm{P}} \in \mathrm{Q}_h^{\mathrm{P}}.\end{aligned}$$

Thus, considering arbitrary $\boldsymbol{\chi}_{\boldsymbol{u},h} \in \mathbf{V}_h$ and $\chi_{p^{\mathrm{P}},h} \in \mathrm{Q}_h^{\mathrm{P}}$, we can deduce from (4.8) with $\vec{\boldsymbol{\theta}}_h = (\vec{\boldsymbol{\chi}}_{\vec{\boldsymbol{\omega}},h} - \vec{\boldsymbol{\omega}}_h) \in \mathrm{Ker}_h(b_1)$ that

$$\begin{aligned}&a((\vec{\boldsymbol{\chi}}_{\vec{\boldsymbol{\omega}},h} - \vec{\boldsymbol{\omega}}_h), (\vec{\boldsymbol{\chi}}_{\vec{\boldsymbol{\omega}},h} - \vec{\boldsymbol{\omega}}_h))\\ &\quad = -a((\vec{\boldsymbol{\omega}} - \vec{\boldsymbol{\chi}}_{\vec{\boldsymbol{\omega}},h}), (\vec{\boldsymbol{\chi}}_{\vec{\boldsymbol{\omega}},h} - \vec{\boldsymbol{\omega}}_h)) - b_1((\vec{\boldsymbol{\chi}}_{\vec{\boldsymbol{\omega}},h} - \vec{\boldsymbol{\omega}}_h), (\boldsymbol{u} - \boldsymbol{\chi}_{\boldsymbol{u},h}))\\ &\qquad - b_1((\vec{\boldsymbol{\chi}}_{\vec{\boldsymbol{\omega}},h} - \vec{\boldsymbol{\omega}}_h), (\boldsymbol{\chi}_{\boldsymbol{u},h} - \boldsymbol{u}_h)) + b_2((\vec{\boldsymbol{\chi}}_{\vec{\boldsymbol{\omega}},h} - \vec{\boldsymbol{\omega}}_h), (p^{\mathrm{P}} - \chi_{p^{\mathrm{P}},h}))\\ &\qquad + b_2((\vec{\boldsymbol{\chi}}_{\vec{\boldsymbol{\omega}},h} - \vec{\boldsymbol{\omega}}_h), (\chi_{p^{\mathrm{P}},h} - p_h^{\mathrm{P}})),\end{aligned}$$

which, together with the ellipticity of $a(\cdot,\cdot)$ and the continuity of $a(\cdot,\cdot)$, $b_1(\cdot,\cdot)$, and $b_2(\cdot,\cdot)$, implies

$$\begin{aligned}(4.11)\qquad \frac{\|\vec{\boldsymbol{\chi}}_{\vec{\boldsymbol{\omega}},h} - \vec{\boldsymbol{\omega}}_h\|_{\mathbf{H}}}{(1+\eta^{\mathrm{P}})} &\leq C_1\{\|\vec{\boldsymbol{\omega}} - \vec{\boldsymbol{\chi}}_{\vec{\boldsymbol{\omega}},h}\|_{\mathbf{H}} + \|\boldsymbol{u} - \boldsymbol{\chi}_{\boldsymbol{u},h}\|_{\mathbf{V}} + \|p^{\mathrm{P}} - \chi_{p^{\mathrm{P}},h}\|_{1,\Omega^{\mathrm{P}}}\}\\ &\quad + \frac{\alpha\|\chi_{p^{\mathrm{P}},h} - p_h^{\mathrm{P}}\|_{0,\Omega^{\mathrm{P}}}}{(\mu^{\mathrm{P}} + \lambda^{\mathrm{P}})(1+\eta^{\mathrm{P}})},\end{aligned}$$

with $C_1 > 0$ independent of h, η^{P}, and η^{E}.

In turn, from (4.10) with $q_h^{\mathrm{P}} = \chi_{p^{\mathrm{P}},h} - p_h^{\mathrm{P}}$, we have

$$\begin{aligned}c((\chi_{p^{\mathrm{P}},h} - p_h^{\mathrm{P}}), (\chi_{p^{\mathrm{P}},h} - p_h^{\mathrm{P}})) &= -c((p^{\mathrm{P}} - \chi_{p^{\mathrm{P}},h}), (\chi_{p^{\mathrm{P}},h} - p_h^{\mathrm{P}}))\\ &\quad - b_3((\vec{\boldsymbol{\chi}}_{\vec{\boldsymbol{\omega}},h} - \vec{\boldsymbol{\omega}}_h), (\chi_{p^{\mathrm{P}},h} - p_h^{\mathrm{P}}))\\ &\quad - b_3((\vec{\boldsymbol{\omega}} - \vec{\boldsymbol{\chi}}_{\vec{\boldsymbol{\omega}},h}), (\chi_{p^{\mathrm{P}},h} - p_h^{\mathrm{P}})).\end{aligned}$$

In this way, applying the ellipticity of $c(\cdot,\cdot)$ and the continuity of $c(\cdot,\cdot)$ and $b_3(\cdot,\cdot)$, we obtain

$$\begin{aligned}&\left[c_0 + \frac{\alpha^2}{(\mu^{\mathrm{P}} + \lambda^{\mathrm{P}})(1+\eta^{\mathrm{P}})}\right]\|\chi_{p^{\mathrm{P}},h} - p_h^{\mathrm{P}}\|_{0,\Omega^{\mathrm{P}}}^2 + \frac{\kappa_1}{\xi}|\chi_{p^{\mathrm{P}},h} - p_h^{\mathrm{P}}|_{1,\Omega^{\mathrm{P}}}^2\\ &\quad \leq C_2\left\{\|\vec{\boldsymbol{\omega}} - \vec{\boldsymbol{\chi}}_{\vec{\boldsymbol{\omega}},h}\|_{\mathbf{H}} + \|(p^{\mathrm{P}} - \chi_{p^{\mathrm{P}},h})\|_{1,\Omega^{\mathrm{P}}}\right\}\|\chi_{p^{\mathrm{P}},h} - p_h^{\mathrm{P}}\|_{1,\Omega^{\mathrm{P}}}\\ &\qquad + \frac{\alpha}{(1+\eta^{\mathrm{P}})}\|\vec{\boldsymbol{\chi}}_{\vec{\boldsymbol{\omega}},h} - \vec{\boldsymbol{\omega}}_h\|_{\mathbf{H}}\|\chi_{p^{\mathrm{P}},h} - p_h^{\mathrm{P}}\|_{0,\Omega^{\mathrm{P}}},\end{aligned}$$

which, together with (4.11), implies

$$\|\chi_{p^{\mathrm{P}},h} - p_h^{\mathrm{P}}\|_{1,\Omega^{\mathrm{P}}} \leq \frac{C_3}{c_1}\left\{\|\vec{\boldsymbol{\omega}} - \vec{\boldsymbol{\chi}}_{\vec{\boldsymbol{\omega}},h}\|_{\mathbf{H}} + \|\boldsymbol{u} - \boldsymbol{\chi}_{\boldsymbol{u},h}\|_{\mathbf{V}} + \|p^{\mathrm{P}} - \chi_{p^{\mathrm{P}},h}\|_{1,\Omega^{\mathrm{P}}}\right\}, \tag{4.12}$$

with $C_3 > 0$ independent of h, η^{P}, and η^{E}.

It is also important to notice that inequalities (4.11) and (4.12) imply that

$$\begin{aligned}\|p^{\mathrm{P}} - p_h^{\mathrm{P}}\|_{1,\Omega^{\mathrm{P}}} &\leq \left(1 + \frac{C_3}{c_1}\right)\|p^{\mathrm{P}} - \chi_{p^{\mathrm{P}},h}\|_{1,\Omega^{\mathrm{P}}} + \frac{C_3}{c_1}\left\{\|\vec{\boldsymbol{\omega}} - \vec{\boldsymbol{\chi}}_{\vec{\boldsymbol{\omega}},h}\|_{\mathbf{H}} + \|\boldsymbol{u} - \boldsymbol{\chi}_{\boldsymbol{u},h}\|_{\mathbf{V}}\right\},\\ \|\vec{\boldsymbol{\omega}} - \vec{\boldsymbol{\omega}}_h\|_{\mathbf{H}} &\leq \left(1 + C_1 + \frac{\alpha C_3}{c_1(\mu^{\mathrm{P}} + \lambda^{\mathrm{P}})}\right)\\ &\qquad \cdot\left\{\|\vec{\boldsymbol{\omega}} - \vec{\boldsymbol{\chi}}_{\vec{\boldsymbol{\omega}},h}\|_{\mathbf{H}} + \|\boldsymbol{u} - \boldsymbol{\chi}_{\boldsymbol{u},h}\|_{\mathbf{V}} + \|p^{\mathrm{P}} - \chi_{p^{\mathrm{P}},h}\|_{1,\Omega^{\mathrm{P}}}\right\}.\end{aligned}$$

Next, by combining the discrete inf-sup condition (4.5), (4.8), and the continuity of $a(\cdot,\cdot)$, $b_1(\cdot,\cdot)$, and $b_2(\cdot,\cdot)$, one readily infers that there exists $C_4 > 0$ independent of h, η^{P}, and η^{E}, such that

(4.13)

$$\begin{aligned}\|\boldsymbol{\chi}_{\boldsymbol{u},h} - \boldsymbol{u}_h\|_{\mathbf{V}} &\leq \widehat{\beta}^{-1}\sup_{\vec{\boldsymbol{\theta}}_h \in \mathbf{H}_h\setminus\mathbf{0}}\frac{|b_1(\vec{\boldsymbol{\theta}}_h, (\boldsymbol{\chi}_{\boldsymbol{u},h} - \boldsymbol{u}_h))|}{\|\vec{\boldsymbol{\theta}}_h\|_{\mathbf{H}}}\\ &= \widehat{\beta}^{-1}\sup_{\vec{\boldsymbol{\theta}}_h \in \mathbf{H}_h\setminus\mathbf{0}}\frac{|a((\vec{\boldsymbol{\omega}} - \vec{\boldsymbol{\omega}}_h), \vec{\boldsymbol{\theta}}_h) + b_1(\vec{\boldsymbol{\theta}}_h, (\boldsymbol{u} - \boldsymbol{\chi}_{\boldsymbol{u},h})) + b_2(\vec{\boldsymbol{\theta}}_h, (p^{\mathrm{P}} - p_h^{\mathrm{P}}))|}{\|\vec{\boldsymbol{\theta}}_h\|_{\mathbf{H}}}\\ &\leq C_4\big(\|\vec{\boldsymbol{\omega}} - \vec{\boldsymbol{\omega}}_h\|_{\mathbf{H}} + \|\boldsymbol{u} - \boldsymbol{\chi}_{\boldsymbol{u},h}\|_{\mathbf{V}} + \|p^{\mathrm{P}} - p_h^{\mathrm{P}}\|_{1,\Omega^{\mathrm{P}}}\big).\end{aligned}$$

Finally, recalling from [20, Theorem 2.6] that

$$\mathrm{dist}(\vec{\boldsymbol{\omega}}, \mathbf{K}_h) \leq \widetilde{C}\mathrm{dist}(\vec{\boldsymbol{\omega}}, \mathbf{H}_h),$$

and by the fact that $\vec{\boldsymbol{\chi}}_{\vec{\boldsymbol{\omega}},h}, \boldsymbol{\chi}_{\boldsymbol{u},h}$, and $\chi_{p^{\mathrm{P}},h}$ are arbitrary, we see that the desired result follows simply by using the triangle inequality and the estimates (4.11)–(4.13). ∎

Finally, approximation properties of the spaces in (4.1) can be found in, e.g., [9, 20]; when these properties are combined with Céa's estimate (4.7), they produce the theoretical rate of convergence of (4.2)–(4.4), summarized in what follows.

THEOREM 4.3. *In addition to the hypotheses of Theorems* 3.1, 4.1, *and* 4.2, *assume that there exists* $s > 0$ *such that* $\boldsymbol{\omega}^{\mathrm{P}} \in \mathbf{H}^s(\Omega^{\mathrm{P}})$, $\boldsymbol{u} \in \mathbf{H}^{1+s}(\Omega)$, $\phi^{\mathrm{P}} \in \mathrm{H}^s(\Omega^{\mathrm{P}})$, $p^{\mathrm{P}} \in \mathrm{H}^{1+s}(\Omega^{\mathrm{P}})$, $\boldsymbol{\omega}^{\mathrm{E}} \in \mathbf{H}^s(\Omega^{\mathrm{E}})$, *and* $p^{\mathrm{E}} \in \mathrm{H}^s(\Omega^{\mathrm{E}})$. *Then, there exists a positive constant* $C_{Conv} > 0$ *independent of* h, η^{P}, *and* η^{E} *such that with the finite element subspaces defined by* (4.1), *there holds*

$$\begin{aligned}&\|\vec{\boldsymbol{\omega}} - \vec{\boldsymbol{\omega}}_h\|_{\mathbf{H}} + \|\boldsymbol{u} - \boldsymbol{u}_h\|_{\mathbf{V}} + \|p^{\mathrm{P}} - p_h^{\mathrm{P}}\|_{1,\Omega^{\mathrm{P}}}\\ &\quad\leq C_{Conv}\, h^{\min\{s,k+1\}}\big(\|\boldsymbol{\omega}^{\mathrm{P}}\|_{s,\Omega^{\mathrm{P}}} + \|\boldsymbol{u}\|_{s+1,\Omega} + \|\phi^{\mathrm{P}}\|_{s,\Omega^{\mathrm{P}}}\\ &\qquad + \|p^{\mathrm{P}}\|_{s+1,\Omega^{\mathrm{P}}} + \|\boldsymbol{\omega}^{\mathrm{E}}\|_{s,\Omega^{\mathrm{E}}} + \|p^{\mathrm{E}}\|_{s,\Omega^{\mathrm{E}}}\big).\end{aligned}$$

4.4. Suggested block structure and computational cost. To close this section we proceed to rewrite the system (4.2)–(4.4) in a double saddle-point structure. For this purpose, we introduce the operators and functionals $\mathcal{A}^{\mathrm{P}} : \mathbf{W}_h^{\mathrm{P}} \times \mathrm{Z}_h^{\mathrm{P}} \to (\mathbf{W}_h^{\mathrm{P}} \times \mathrm{Z}_h^{\mathrm{P}})'$, $\mathcal{B}_1^{\mathrm{P}} : \mathbf{W}_h^{\mathrm{P}} \times \mathrm{Z}_h^{\mathrm{P}} \to (\mathbf{V}_h)'$, $\mathcal{B}_2^{\mathrm{P}} : \mathrm{Q}_h^{\mathrm{P}} \to (\mathbf{W}_h^{\mathrm{P}} \times \mathrm{Z}_h^{\mathrm{P}})'$, $\mathcal{B}_3^{\mathrm{P}} : \mathbf{W}_h^{\mathrm{P}} \times \mathrm{Z}_h^{\mathrm{P}} \to$

$(\mathrm{Q}_h^{\mathrm{P}})'$, $\mathcal{A}^{\mathrm{E}} : \mathbf{W}_h^{\mathrm{E}} \times \mathrm{Q}_h^{\mathrm{E}} \to (\mathbf{W}_h^{\mathrm{E}} \times \mathrm{Q}_h^{\mathrm{E}})'$, $\mathcal{B}_1^{\mathrm{E}} : \mathbf{W}_h^{\mathrm{E}} \times \mathrm{Q}_h^{\mathrm{E}} \to (\mathbf{V}_h)'$, $\mathcal{C} : \mathrm{Q}_h^{\mathrm{P}} \to (\mathrm{Q}_h^{\mathrm{P}})'$, $\mathcal{F}^{\mathrm{P}}$, $\mathcal{F}^{\mathrm{E}} \in (\mathbf{V}_h)'$, $\mathcal{G} \in (\mathrm{Q}_h^{\mathrm{P}})'$, which are specified as

$$
\begin{aligned}
[\mathcal{A}^{\mathrm{P}}(\boldsymbol{\omega}_h^{\mathrm{P}}, \phi_h^{\mathrm{P}}), (\boldsymbol{\theta}_h^{\mathrm{P}}, \psi_h^{\mathrm{P}})] &:= \int_{\Omega^{\mathrm{P}}} \boldsymbol{\omega}_h^{\mathrm{P}} \cdot \boldsymbol{\theta}_h^{\mathrm{P}} + \frac{1}{1+\eta^{\mathrm{P}}} \int_{\Omega^{\mathrm{P}}} \phi_h^{\mathrm{P}} \psi_h^{\mathrm{P}}, \\
[\mathcal{A}^{\mathrm{E}}(\boldsymbol{\omega}_h^{\mathrm{E}}, p_h^{\mathrm{E}}), (\boldsymbol{\theta}_h^{\mathrm{E}}, q_h^{\mathrm{E}})] &:= \int_{\Omega^{\mathrm{E}}} \boldsymbol{\omega}_h^{\mathrm{E}} \cdot \boldsymbol{\theta}_h^{\mathrm{E}} + \int_{\Omega^{\mathrm{E}}} p_h^{\mathrm{E}} q_h^{\mathrm{E}}, \\
[\mathcal{B}_1^{\mathrm{P}}(\boldsymbol{\theta}_h^{\mathrm{P}}, \psi_h^{\mathrm{P}}), \boldsymbol{v}_h] &:= -\sqrt{\eta^{\mathrm{P}}} \int_{\Omega^{\mathrm{P}}} \boldsymbol{\theta}_h^{\mathrm{P}} \cdot \mathbf{curl}\, \boldsymbol{v}_h + \int_{\Omega^{\mathrm{P}}} \psi_h^{\mathrm{P}} \operatorname{div} \boldsymbol{v}_h, \\
[\mathcal{B}_1^{\mathrm{E}}(\boldsymbol{\theta}_h^{\mathrm{E}}, q_h^{\mathrm{E}}), \boldsymbol{v}_h] &:= -\sqrt{\eta^{\mathrm{E}}} \int_{\Omega^{\mathrm{E}}} \boldsymbol{\theta}_h^{\mathrm{E}} \cdot \mathbf{curl}\, \boldsymbol{v}_h + \int_{\Omega^{\mathrm{E}}} q_h^{\mathrm{E}} \operatorname{div} \boldsymbol{v}_h, \\
[\mathcal{B}_2^{\mathrm{P}}(\boldsymbol{\theta}_h^{\mathrm{P}}, \psi_h^{\mathrm{P}}), p_h^{\mathrm{P}}] &:= \frac{\alpha}{(1+\eta^{\mathrm{P}})(\lambda^{\mathrm{P}} + \mu^{\mathrm{P}})} \int_{\Omega^{\mathrm{P}}} p_h^{\mathrm{P}} \psi_h^{\mathrm{P}}, \\
[\mathcal{B}_3^{\mathrm{P}}(\boldsymbol{\omega}_h^{\mathrm{P}}, \phi_h^{\mathrm{P}}), q_h^{\mathrm{P}}] &:= \frac{\alpha}{(1+\eta^{\mathrm{P}})} \int_{\Omega^{\mathrm{P}}} q_h^{\mathrm{P}} \phi_h^{\mathrm{P}}, \\
[\mathcal{C}(p_h^{\mathrm{P}}), q_h^{\mathrm{P}}] &:= \left[c_0 + \frac{\alpha^2}{(\mu^{\mathrm{P}} + \lambda^{\mathrm{P}})(1+\eta^{\mathrm{P}})} \right] \int_{\Omega^{\mathrm{P}}} p_h^{\mathrm{P}} q_h^{\mathrm{P}} + \frac{1}{\xi} \int_{\Omega^{\mathrm{P}}} \kappa \nabla p_h^{\mathrm{P}} \cdot \nabla q_h^{\mathrm{P}}, \\
[\mathcal{F}^{\mathrm{P}}, (\boldsymbol{v}_h)] &:= -\int_{\Omega^{\mathrm{P}}} \boldsymbol{f}^{\mathrm{P}} \cdot \boldsymbol{v}_h, \quad [\mathcal{F}^{\mathrm{E}}, (\boldsymbol{v}_h)] := -\int_{\Omega^{\mathrm{E}}} \boldsymbol{f}^{\mathrm{E}} \cdot \boldsymbol{v}_h, \\
[\mathcal{G}, (q_h^{\mathrm{P}})] &:= -\frac{\rho}{\xi} \int_{\Omega^{\mathrm{P}}} \kappa \boldsymbol{g} \cdot \nabla q_h^{\mathrm{P}} - \int_{\Omega^{\mathrm{P}}} s q_h^{\mathrm{P}},
\end{aligned}
$$

and arrive at the following double saddle-point Galerkin scheme:

$$
\left[\begin{array}{cc:c:c}
\mathcal{A}^{\mathrm{P}} & 0 & (\mathcal{B}_1^{\mathrm{P}})' & -\mathcal{B}_2^{\mathrm{P}} \\
0 & \mathcal{A}^{\mathrm{E}} & (\mathcal{B}_1^{\mathrm{E}})' & \mathbf{0} \\
\hdashline
\mathcal{B}_1^{\mathrm{P}} & \mathcal{B}_1^{\mathrm{E}} & \mathbf{0} & \mathbf{0} \\
\hdashline
\mathcal{B}_3^{\mathrm{P}} & \mathbf{0} & \mathbf{0} & -\mathcal{C}
\end{array}\right]
\left[\begin{array}{c}
(\boldsymbol{\omega}_h^{\mathrm{P}}, \phi_h^{\mathrm{P}}) \\
(\boldsymbol{\omega}_h^{\mathrm{E}}, p_h^{\mathrm{E}}) \\
\boldsymbol{u}_h \\
p_h^{\mathrm{P}}
\end{array}\right]
=
\left[\begin{array}{c}
\mathbf{0} \\
\mathbf{0} \\
\mathcal{F}^{\mathrm{P}} + \mathcal{F}^{\mathrm{E}} \\
\mathcal{G}
\end{array}\right],
\tag{4.14}
$$

which is precisely the way that the implementation is carried out. From this system it is clear that the coupling occurs only through the global displacement blocks. Notice also that (4.14) could be analyzed using Fredholm's alternative theory in combination with an extension of the Babuška–Brezzi theory for multiple saddle-point problems [21, 30] (see, e.g., [32]).

Regarding the computational cost of the formulation, the proposed scheme is still competitive even if the formulation includes additional variables. Considering, for illustrative purposes, the 2D case, and denoting by $N_v^\star, N_T^\star, N_l^\star$ the number of vertices, triangles, and edges associated with a triangulation for the generic subdomain $\star \in \{\mathrm{E}, \mathrm{P}\}$, a simple computation of the required degrees of freedom (DoFs) in (4.14) (and restricting to the lowest-order case) is

$$
2N_T^{\mathrm{P}} + 3N_v^{\mathrm{P}} + 2N_T^{\mathrm{E}} + 2N_v^{\mathrm{E}} \approx 7N_v^{\mathrm{P}} + 6N_v^{\mathrm{E}}.
$$

On the other hand, we remark that more classical methods for the coupling of elasticity and poroelasticity, without including rotations and still possessing the locking-free property, seem to be unavailable in the literature. But one could employ MINI elements to approximate displacement and hydrostatic pressure in the elastic domain while using the formulation from [38] for the Biot poroelasticity, with either Taylor–Hood + Lagrange in the poroelastic domain

$$
4N_v^{\mathrm{P}} + 2N_l^{\mathrm{P}} + 3N_v^{\mathrm{E}} + 2N_T^{\mathrm{E}} \approx 10N_v^{\mathrm{P}} + 7N_v^{\mathrm{E}},
$$

or

MINI elements + Lagrange in the poroelastic domain

$$6N_v^{\mathrm{P}} + 2N_l^{\mathrm{P}} + 3N_v^{\mathrm{E}} + 2N_T^{\mathrm{E}} \approx 8N_v^{\mathrm{P}} + 7N_v^{\mathrm{E}},$$

which are both more costly than (4.14). Furthermore, other rotation-based formulations that could generate robust schemes are typically based on much more expensive forms using rotation tensors, displacement gradients, or stress tensors in addition to displacement and pressure.

5. Computational examples. In this section we address the numerical verification of the convergence properties of the proposed schemes as well as the usability of these methods in a problem of more applicative interest. The solution of all linear systems in the form (4.14) and reported in this section has been conducted with the Krylov method flexible GMRES, preconditioned with additive Schwarz using incomplete LU decomposition as local preconditioner.

Test 1: Convergence verification. First, we construct a sequence of successively refined uniform partitions of the elastic domain $\Omega = (0,1)^2$. The poroelastic region is $\Omega^{\mathrm{P}} = (0.25, 0.75)^2$, and the geometric setup is exemplified (for a coarse mesh) in the top-left panel of Figure 5.1. A closed-form solution for the global displacement satisfying (2.11) is

$$\boldsymbol{u}(x,y) = u_{\max} \begin{pmatrix} x(1-x)\cos(\pi x)\sin(2\pi y) \\ \sin(\pi x)\cos(\pi y) y^2(1-y) \end{pmatrix}, \tag{5.1}$$

where we use $u_{\max} = 0.1$. A material interface is considered between the two regions, and so we impose a jump in the Young modulus and Poisson ratios of the solids $E^{\mathrm{P}} = 100$, $E^{\mathrm{E}} = 10000$, $\nu^{\mathrm{P}} = 0.3$, $\nu^{\mathrm{E}} = 0.45$. Consequently, the exact rotations will have different scalings in each domain. The remaining closed-form solutions and model constants are taken as follows:

(5.2)
$$p^{\mathrm{E}} = -\operatorname{div} \boldsymbol{u}, \quad p^{\mathrm{P}}(x,y) = \sin(\pi x)\sin(\pi y), \quad \phi^{\mathrm{P}} = \alpha(\lambda^{\mathrm{P}} + \mu^{\mathrm{P}})^{-1} p^{\mathrm{P}} - (1+\eta^{\mathrm{P}}) \operatorname{div} \boldsymbol{u},$$
$$\boldsymbol{g} = \boldsymbol{0}, \quad \kappa = 10^{-6}, \quad \alpha = 0.1, \quad \xi = 10^{-2}, \quad c_0 = 10^{-3}.$$

The source terms (and, for this example, the remainders of the exact fluxes and traction forces on the interface) are imposed using these exact solutions. In Table 5.1 we collect the computed errors on each refinement level, separating each individual contribution to the errors in $\mathbf{H}$; that is, we show

$$e(\boldsymbol{\omega}^{\mathrm{P}}) := \|\boldsymbol{\omega}^{\mathrm{P}} - \boldsymbol{\omega}_h^{\mathrm{P}}\|_{0,\Omega^{\mathrm{P}}}, \quad e(\phi^{\mathrm{P}}) := \|\phi^{\mathrm{P}} - \phi_h^{\mathrm{P}}\|_{0,\Omega^{\mathrm{P}}}, \quad e(\boldsymbol{\omega}^{\mathrm{E}}) := \|\boldsymbol{\omega}^{\mathrm{E}} - \boldsymbol{\omega}_h^{\mathrm{E}}\|_{0,\Omega^{\mathrm{E}}},$$
$$e(p^{\mathrm{E}}) := \|p^{\mathrm{E}} - p_h^{\mathrm{E}}\|_{0,\Omega^{\mathrm{E}}}, \quad e(\boldsymbol{u}) := \|\boldsymbol{u} - \boldsymbol{u}_h\|_{\mathbf{V}}, \quad e(p^{\mathrm{P}}) := \|p^{\mathrm{P}} - p_h^{\mathrm{P}}\|_{1,\Omega^{\mathrm{P}}}$$

as well as the corresponding decay trend, $\texttt{rate} = \log\big(e(\cdot)/\widehat{e}(\cdot)\big)[\log(h/\widehat{h})]^{-1}$, where $e, \widehat{e}$ stand for errors generated on meshes with mesh sizes h and $\widehat{h}$, respectively. For this 2D problem, the tabulated results in the upper two blocks of the table are produced using the finite element spaces specified in (4.1) for $k = 0$ and $k = 1$, and they demonstrate numerically the optimal convergence order anticipated by Theorem 4.3.

A similar conclusion is drawn when testing the accuracy of the 3D implementation. In that case, we define the domain as the unit cube $\Omega = (0,1)^3$ and take the poroelastic

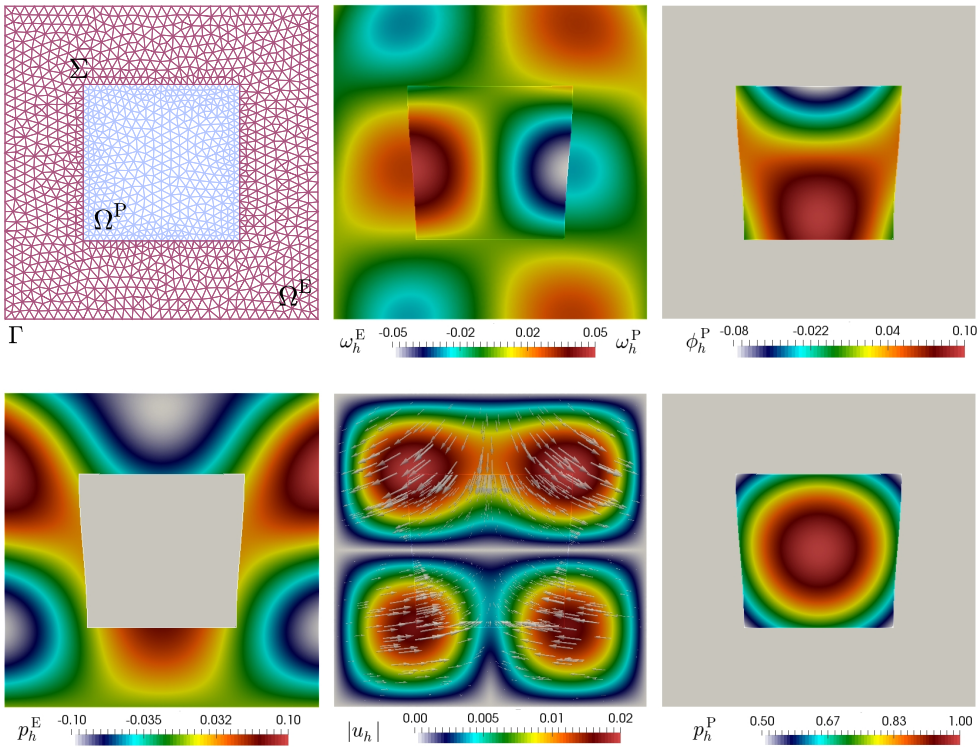


FIG. 5.1. *Test* 1. *Sketched mesh and domains before deformation (top left) and approximate solutions generated with a second-order scheme and plotted on the deformed configuration: rotations on each domain (top middle), total poroelastic pressure (top right), elastic pressure (bottom left), global displacement magnitude (bottom middle), and poroelastic fluid pressure (bottom right).*

region as the embedded inner cube $\Omega^{\mathrm{P}} = (0.25, 0.75)^3$. The manufactured global displacement and fluid poroelastic pressure solutions are the smooth functions

$$\boldsymbol{u}(x,y,z) = \begin{pmatrix} \sin^2(\pi x)\sin(\pi x)\sin(2\pi z) \\ \sin(\pi x)\sin^2(\pi x)\sin(2\pi z) \\ -(\sin(2\pi x)\sin(\pi y) + \sin(\pi x)\sin(2\pi y))\sin^2(\pi z) \end{pmatrix}, \tag{5.3}$$
$$p^{\mathrm{P}}(x,y,z) = \sin(\pi x)\sin(\pi y)\sin(\pi z),$$

which are used to construct the remaining unknowns as well as the data. All other model constants are assumed as in the previous 2D case. The bottom two blocks of Table 5.1 also show optimal decay rates, exhibiting behavior consistent with the theoretical findings.

Test 2: Validation using augmented Mandel's problem. Second, we conduct a benchmark test for poromechanics. We solve the classical Mandel's problem, here extended to the case of coupled elastic-poroelastic structures following the configuration and parameter values from [27, 45]. The values of the constants are taken to be

$$c_0 = 2.5\text{e-}12\,\mathrm{Pa}^{-1}, \quad \alpha = 1, \quad \xi = 10^{-3}\mathrm{m}^2/s, \quad \mu^{\mathrm{E}} = \mu^{\mathrm{P}} = 10^8\,\mathrm{Pa}, \quad \nu^{\mathrm{E}} = \nu^{\mathrm{P}} = 0.2,$$
$$\kappa = 10^{-13}\,\mathrm{m}^2, \quad \rho = 1\,\mathrm{Kg/m}^3, \quad \widetilde{\boldsymbol{t}} = (0, -10^7)^{\mathrm{t}}\,\mathrm{Pa}\cdot\mathrm{m}.$$

TABLE 5.1

Test 1. *Error history demonstrating the convergence predicted by Theorem* 4.3*, here illustrated for first- and second-order schemes and for* 2*D and* 3*D tests.*

h	$e(\boldsymbol{\omega}^{\mathrm{P}})$	rate	$e(\phi^{\mathrm{P}})$	rate	$e(\boldsymbol{\omega}^{\mathrm{E}})$	rate	$e(p^{\mathrm{E}})$	rate	$e(\boldsymbol{u})$	rate	$e(p^{\mathrm{P}})$	rate
2D scheme using $k=0$ and the exact solutions (5.1)–(5.2)												
0.195	4.44e-3	–	8.73e-3	–	4.53e-3	–	1.27e-2	–	1.55e-2	–	2.34e-1	–
0.175	3.03e-3	2.531	4.85e-3	2.430	4.33e-3	0.428	1.16e-3	0.831	1.32e-2	1.470	1.16e-1	1.520
0.089	1.84e-3	0.838	2.90e-3	0.754	2.17e-3	1.020	6.02e-3	0.971	6.97e-3	0.945	6.48e-2	0.853
0.047	9.75e-4	0.889	1.63e-3	0.905	1.11e-3	1.051	3.02e-3	1.091	3.56e-3	1.061	3.49e-2	0.973
0.024	5.29e-4	0.998	8.28e-4	0.988	5.62e-4	0.992	1.54e-3	0.973	1.83e-3	0.972	1.84e-2	0.985
0.012	2.31e-4	1.170	5.41e-4	0.902	2.82e-4	0.997	7.54e-4	1.016	9.22e-4	0.963	9.59e-3	0.915
0.006	1.30e-5	0.835	2.47e-4	1.130	1.39e-4	1.034	3.73e-4	1.023	4.54e-4	1.030	4.92e-3	0.968
0.003	6.56e-6	0.962	1.23e-4	1.004	6.92e-5	1.003	1.85e-4	1.015	2.25e-4	1.022	2.48e-3	0.977
2D scheme using $k=1$ and the exact solutions (5.1)–(5.2)												
0.195	8.51e-4	–	1.39e-3	–	8.36e-4	–	1.56e-3	–	2.24e-2	–	1.98e-1	–
0.175	2.40e-4	2.721	3.61e-4	2.402	6.06e-4	2.972	1.10e-3	3.225	1.31e-3	2.835	3.76e-2	2.504
0.089	7.58e-5	1.750	1.22e-4	1.692	1.55e-4	2.013	2.80e-4	2.014	3.40e-4	1.987	1.06e-2	1.686
0.047	2.57e-5	1.812	4.16e-5	1.769	4.13e-5	2.086	7.63e-5	2.040	9.53e-5	2.005	3.41e-3	1.759
0.024	7.52e-6	1.880	1.15e-5	1.987	1.01e-5	2.053	1.96e-5	1.981	2.47e-5	1.963	1.03e-4	1.798
0.012	1.88e-6	1.951	3.40e-6	1.972	2.50e-6	1.971	4.85e-6	1.973	6.26e-6	1.948	2.68e-5	1.896
0.006	4.81e-7	1.964	8.57e-7	1.983	6.07e-7	2.016	1.22e-6	1.998	1.52e-6	1.975	7.76e-6	1.952
3D scheme using $k=0$ and the exact solutions (5.3)												
0.433	0.892	–	0.477	–	0.781	–	1.042	–	1.619	–	8.721	–
0.289	0.629	0.860	0.407	0.639	0.404	0.631	0.561	0.940	0.842	0.847	4.480	0.889
0.296	0.422	0.963	0.299	0.896	0.278	0.881	0.270	0.962	0.425	0.915	2.246	0.953
0.185	0.338	0.975	0.237	0.950	0.192	0.967	0.136	0.938	0.228	0.926	1.104	1.029
0.098	0.393	0.986	0.174	0.995	0.095	1.012	0.078	0.992	0.119	0.994	0.545	1.017
3D scheme using $k=1$ and the exact solutions (5.3)												
0.433	0.447	–	0.286	–	0.437	–	0.510	–	0.832	–	7.833	–
0.289	0.135	1.785	0.104	1.502	0.138	1.491	0.159	1.482	0.309	1.595	2.281	1.713
0.296	3.51e-3	1.864	2.66e-2	1.765	3.56e-2	1.864	4.05e-2	1.933	7.69e-2	1.873	0.607	1.805
0.185	9.11e-4	1.878	6.67e-3	1.938	1.06e-2	1.895	1.04e-2	1.968	2.06e-2	1.886	0.159	1.909
0.098	2.35e-4	1.992	1.74e-3	1.986	2.65e-3	1.983	2.66e-3	1.980	5.10e-3	1.951	4.12e-2	1.974

For this problem the goal is to observe the so-called Mandel–Creyer effect, where the fluid pressure increases with time and then decreases over the poroelastic region. The elastic domain $\Omega^{\mathrm{E}} = (0, 100) \times (20, 40)\,\mathrm{m}^2$ is located on top of the poroelastic region $\Omega^{\mathrm{P}} = (0, 100) \times (0, 20)\,\mathrm{m}^2$, as shown in the schematic illustration of Figure 5.2 (left). The boundary conditions adopted for this test differ from (2.11). On the top of the elastic domain Γ^{top} we prescribe a constant traction $\widetilde{\boldsymbol{t}}$; on the right end of the elastic domain we set zero traction; on the left of the elastic and poroelastic domains and on the bottom of the poroelastic domain we enforce a zero normal displacement; and on the right of the poroelastic domain we put $p^{\mathrm{P}} = 0$, whereas we impose $\kappa \nabla p^{\mathrm{P}} \cdot \boldsymbol{n} = 0$ on the left and bottom of the poroelastic domain. We do not include gravitational effects for this test. Note that traction boundary conditions can be incorporated into the context of rotation-based formulations by means of the additional term

$$[\mathcal{A}^{\boldsymbol{u}}(\boldsymbol{u}_h), \boldsymbol{v}_h] = \langle 2\eta^{\mathrm{E}} \nabla \boldsymbol{u}_h \boldsymbol{n}, \boldsymbol{v}_h \rangle_{\Gamma^{\mathrm{top}} \cup \Gamma^{\mathrm{E}}_{\mathrm{right}}} + \langle 2 \operatorname{div} \boldsymbol{u}_h \boldsymbol{n}, \boldsymbol{v}_h \rangle_{\Gamma^{\mathrm{top}} \cup \Gamma^{\mathrm{E}}_{\mathrm{right}}} \tag{5.4}$$

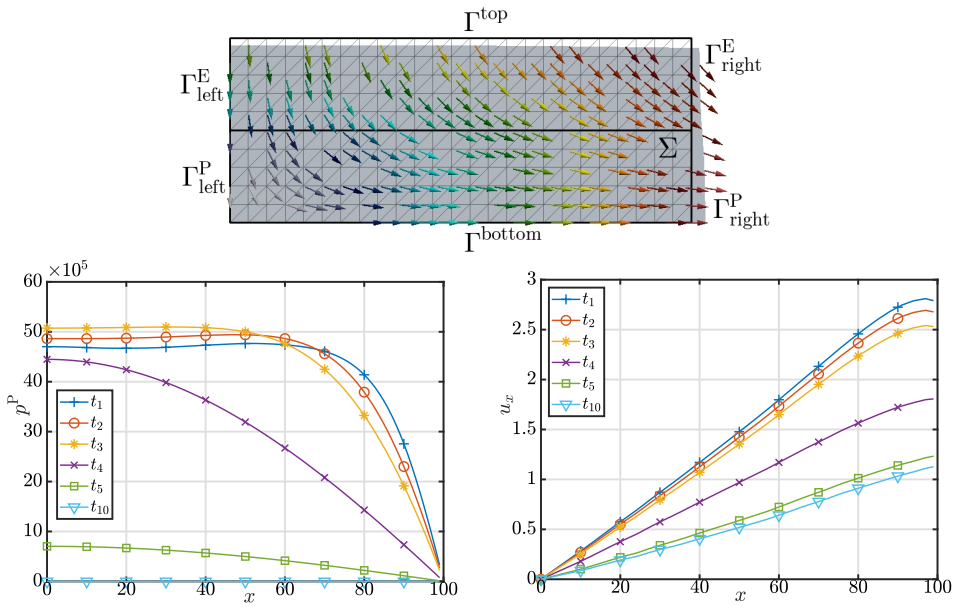


FIG. 5.2. *Test 2. Sample coarse mesh and domain/boundary configuration (top), and profiles of fluid pressure and x-displacement on* Γ^{bottom} *(bottom) at different times* ($t_1 = 10^3$ *s*, $t_2 = 5e3$ *s*, $t_3 = 10^4$ *s*, $t_4 = 10^5$ *s*, $t_5 = 5e5$ *s*, $t_{10} = 5e6$ *s*) *for the augmented Mandel's problem.*

for the 2D case, or

$$[\mathcal{A}^{\boldsymbol{u}}(\boldsymbol{u}_h), \boldsymbol{v}_h] = -\langle 2\eta^{\text{E}} \nabla \boldsymbol{u}_h \boldsymbol{n}, \boldsymbol{v}_h \rangle_{\Gamma^{\text{top}} \cup \Gamma^{\text{E}}_{\text{right}}} + \langle 2\eta^{\text{E}} \operatorname{div} \boldsymbol{u}_h \boldsymbol{n}, \boldsymbol{v}_h \rangle_{\Gamma^{\text{top}} \cup \Gamma^{\text{E}}_{\text{right}}} \tag{5.5}$$

in 3D, as part of the corresponding displacement block in (4.14) (see further details in [4, sect. 3.2]), and adding the term

$$\langle \boldsymbol{t}, \boldsymbol{v}_h \rangle_{\Gamma^{\text{top}} \cup \Gamma^{\text{E}}_{\text{right}}} \quad \text{or} \quad -\langle \boldsymbol{t}, \boldsymbol{v}_h \rangle_{\Gamma^{\text{top}} \cup \Gamma^{\text{E}}_{\text{right}}}$$

in 2D or 3D, respectively, into $\mathcal{F}^{\text{E}}$, appearing on the right-hand side of (4.14), with $\boldsymbol{t} := \widetilde{\boldsymbol{t}}/(\mu^{\text{E}} + \lambda^{\text{E}})$. Similar terms can be derived to impose traction conditions for the rotation-based formulation of the poroelasticity equation (2.13). Moreover, for simplicity when imposing traction conditions, in the present example we have used in both the elastic and poroelastic domains the same scaling $\eta^{\text{E}} = \eta^{\text{P}}$, and consequently on the right-hand sides we have the rescaling $1/(\mu^{\text{E}} + \lambda^{\text{E}}) = 1/(\mu^{\text{P}} + \lambda^{\text{P}})$. We use a structured triangular mesh and a first-order numerical scheme (setting $k = 0$ in the finite element spaces (4.1)).

Note that we also incorporate time-dependence into the mass conservation equation (2.1), in the first two terms of the left-hand side,

$$\begin{aligned} &\left[c_0 + \alpha^2(\mu^{\text{P}} + \lambda^{\text{P}})^{-1}(1 + \eta^{\text{P}})^{-1}\right]\partial_t p^{\text{P}} - \alpha(1 + \eta^{\text{P}})^{-1}\partial_t \phi^{\text{P}} \\ &\qquad -\frac{1}{\xi} \operatorname{div}\left[\kappa(\nabla p^{\text{P}} - \rho \boldsymbol{g})\right] = 0 \quad \text{in } \Omega^{\text{P}} \times (0, t_{\text{final}}], \end{aligned}$$

with initial conditions given by $p^{\text{P}}(0) = 0$ and $\phi^{\text{P}}(0) = 0$. This turns the poroelasticity equations into their quasi-steady regime, and we therefore discretize in time

and use a backward Euler scheme, setting a fixed time step $\Delta t = 1000\,\mathrm{s}$ and running the simulation for 5000 steps. We record fluid pressure profiles as well as horizontal displacements at different time instants and collect the results in the plots of Figure 5.2 (bottom panels). Even if the value of the maximal horizontal displacement is lower than that reported in [27, 45] (which can be explained by the differences in transmission conditions, in the problem formulation, in the polynomial degree of the numerical schemes, and in mesh resolution), qualitatively we observe the expected behavior in fluid pressure profiles and motion patterns.

Test 3: Poroelastic aquifer in 3D. Next, we solve a 3D problem similar to that described in [25], where one is interested in determining deformation and fluid pressure distribution of the pay zone (a poroelastic aquifer region occupying $\Omega^{\mathrm{P}} = (-225, 225) \times (-225, 225) \times (-30, 30)\,\mathrm{m}^3$) surrounded by rock conforming the nonpay zone (an elastic, nonporous structure $\Omega^{\mathrm{E}} = (-450, 450) \times (-450, 450) \times (-150, 150)\,\mathrm{m}^3$). The scenario corresponds to coupled flow and poromechanics encountered in CO_2 sequestration in deep subsurface reservoirs. A localized source $s^{\mathrm{P}}(x, y, z) = s_0 \exp(-(x-225)^2 - (y-225)^2)$ represents an injection zone of relatively small radius reaching the top corner of the pay zone. On the top surface of the pay rock, Γ^{top}, we assume zero traction, using the technique described in (5.5). On the remainder of Γ, we impose the sliding condition

$$\boldsymbol{u} \cdot \boldsymbol{n} = 0 \quad \text{on } \Gamma \setminus \Gamma^{\mathrm{top}}.$$

Interface conditions are precisely as in (2.12), and we impose a smooth body load on the nonpay rock $\boldsymbol{f}^{\mathrm{E}} = f_0(\sin(f_1 x)\sin(f_1 y), \cos(f_1 y)\cos(f_1 z), \frac{1}{2}\sin(f_1 z)\cos(f_1 x))^{\mathtt{t}}$. We now consider gravitational effects and take a relatively large permeability. The remaining parameters assume the values

$$\begin{gathered} s_0 = 1.8\text{e-}3, \quad f_0 = 10^{-3}, \quad f_1 = 7.5\text{e-}3, \quad \alpha = 0.8, \quad \rho = 1, \\ E^{\mathrm{E}} = E^{\mathrm{P}} = 3.4474\text{e+}9\,\mathrm{Pa}, \\ \nu^{\mathrm{E}} = 0.45, \quad \nu^{\mathrm{P}} = 0.2, \quad \xi = 10^{-3}\,\mathrm{Pa\ s}, \\ \kappa = 9.869\text{e-}9\,\mathrm{m}^2, \quad c_0 = 6.060\text{e-}5, \quad \boldsymbol{g} = (0, 0, -9.81)^{\mathtt{t}}. \end{gathered}$$

The domain is discretized with a rather coarse tetrahedral mesh, and we employ a first-order scheme. From Figure 5.3 we observe an important deformation of the rock and the pay zone, as well as a fluid pressure propagating from the location of the injection well towards the opposite corner of the reservoir.

Test 4: Coupling of tooth and periodontal ligament. We continue with the simulation of distributed forces in a dentistry-oriented application. The problem setup is adapted from that in [18], where one considers the coupling between the tooth as an elastic structure and the surrounding periodontal ligament regarded as a poroelastic material. In this case, however, we assume that the volume fractions in both regions coincide and that the fluid viscosity and density of each phase remain constant. The motivating example from [18] concentrates on determining displacement and stress behavior of the composite material when a piezoelectric actuator applies an external load on the center of the labial side of the crown of a two-rooted premolar in a porcine jawbone segment (the location is illustrated with a sphere in the top-left panel of Figure 5.4). A relatively coarse tetrahedral mesh is used for both domains, and the boundary conditions are set in the following way. We assume that the external surface of the periodontal ligament, Γ^{P}, is in contact with the jawbone, and therefore we set zero solid displacements and zero-flux conditions for the fluid pressure. On the visible

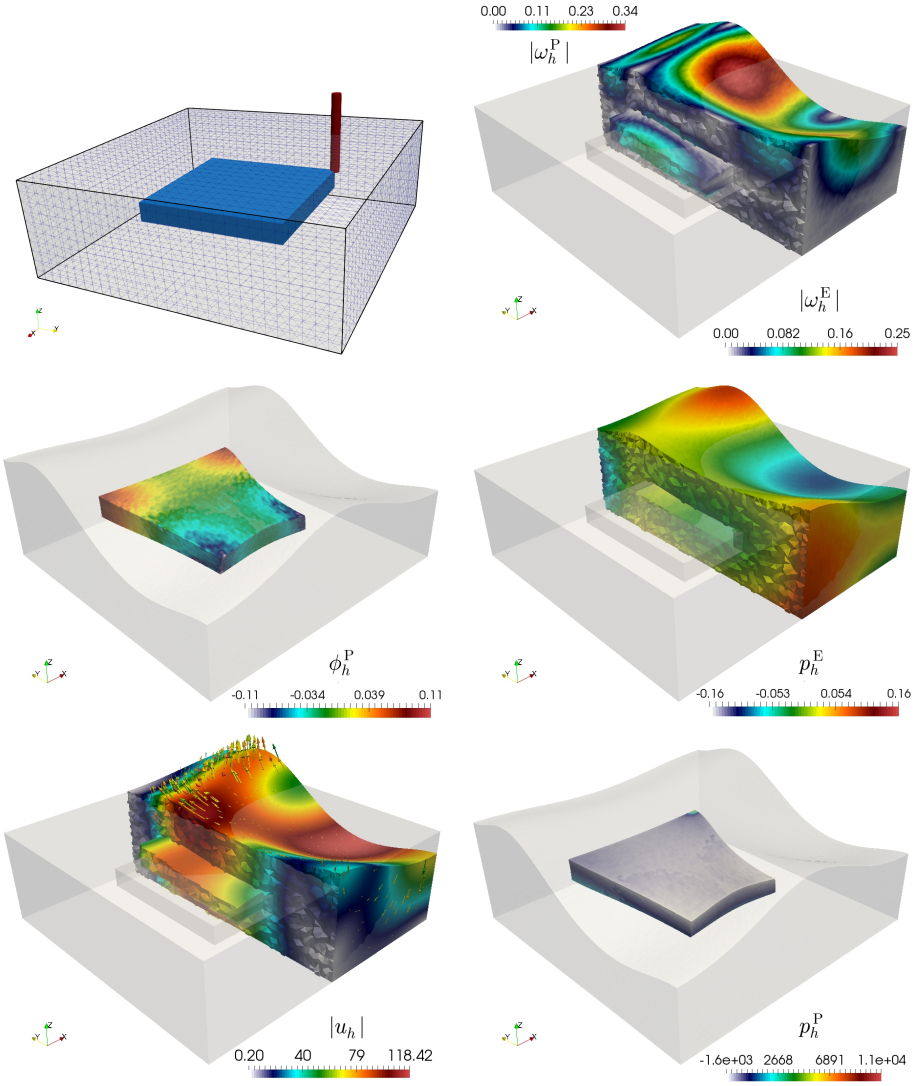


FIG. 5.3. *Test* 3. *Meshes associated with the confined reservoir* Ω^{P} *and the surrounding nonpay rock* Ω^{E} *(top left, sketching also the location of the injection well), and samples of approximate solutions generated with a first-order method.*

part of the tooth, Γ^{E}, we impose the traction $\boldsymbol{t} = \frac{t_{\max}}{\lambda^{\mathrm{E}}+2\mu^{\mathrm{E}}}\chi|_{\mathrm{load}}$, where $\chi|_{\mathrm{load}}$ is the indicator function on a ball of radius 10 mm centered at $(200, 15, 60)$. Again, the interface conditions on Σ are set as in (2.12). The body loads in both domains are $\boldsymbol{f}^{\mathrm{E}} = \frac{\rho^{\mathrm{E}}}{\lambda^{\mathrm{E}}+2\mu^{\mathrm{E}}}\boldsymbol{g}$ and $\boldsymbol{f}^{\mathrm{P}} = \frac{\rho^{\mathrm{P,s}}+\rho^{\mathrm{P,f}}}{\lambda^{\mathrm{P}}+\mu^{\mathrm{P}}}\boldsymbol{g}$, and the rest of the model parameters are set as

$$
\begin{gathered}
s_0 = 0, \quad c_0 = 10^{-3}, \quad t_{\max} = 0.016, \quad \alpha = 0.4, \\
\rho^{\mathrm{E}} = 6000, \quad \rho^{\mathrm{P,s}} = 1060, \quad \rho^{\mathrm{P,f}} = 1000, \\
E^{\mathrm{E}} = 2\mathrm{e}5, \quad E^{\mathrm{P}} = 2\mathrm{e}10, \quad \nu^{\mathrm{E}} = 0.3, \quad \nu^{\mathrm{P}} = 0.31, \\
\xi = 1, \quad \kappa = 10^{-6}\mathrm{mm}^2, \quad \boldsymbol{g} = (0, 0, -9.81)^{\mathrm{t}}.
\end{gathered}
$$

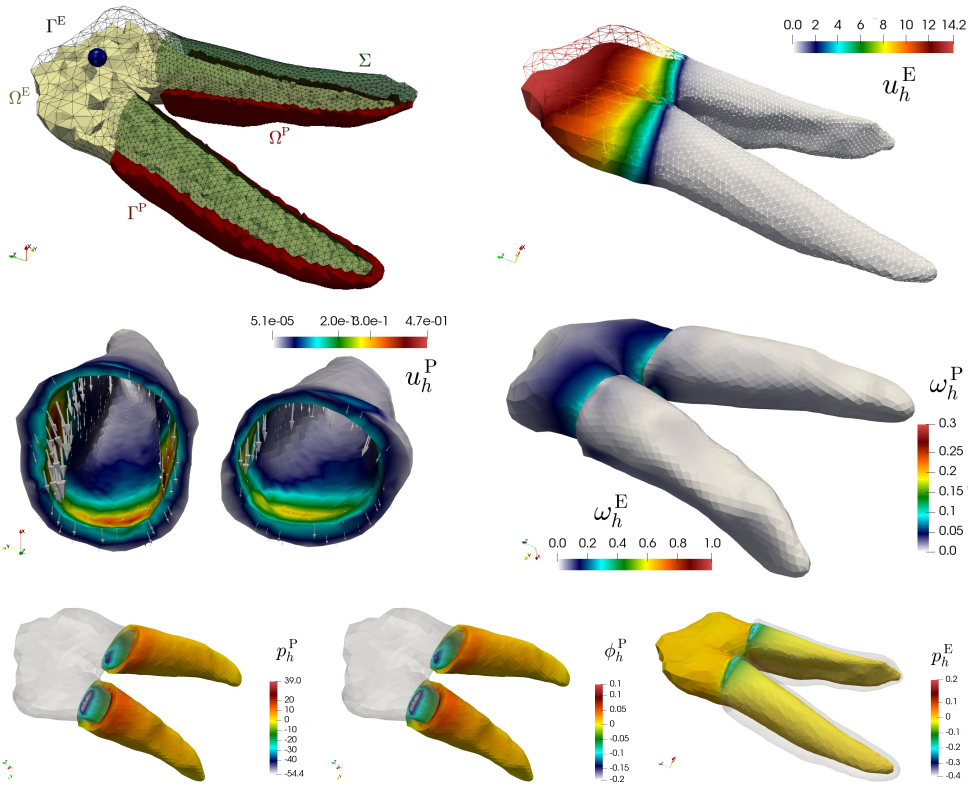


FIG. 5.4. *Test* 4. *Meshes associated with the periodontal ligament* Ω^{P} *and a porcine premolar specimen* Ω^{E} *(top left, sketching also the location of the applied load,* 19 *mm away from the root), and samples of approximate solutions generated with a second-order method.*

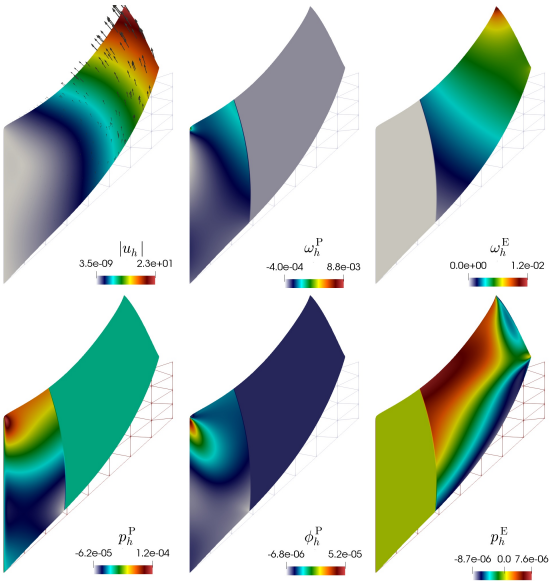
Figure 5.4 reveals zones of concentrated solid pressure near the upper part of Σ, and we notice also high gradients of fluid pressure in neighboring areas, all consistent with the results reported in [18].

Test 5: Robustness with respect to the Poisson ratio. To finish this section we conduct a series of computations to test the locking-free property of the method. We simply examine the mechanical response of a composite material and compute solutions of an appropriate adaptation of the classical Cook's membrane test, where we study elastic response dominated by bending and shear. The extension of this benchmark to poromechanics was recently carried out in [44], whereas a rotation-based formulation was tested in [4]. The domain Ω is the convex hull of the set $\{(0,0),(\ell,w),(\ell,\ell+s),(0,w)\}$, with $\ell = 48$, $w = 44$, $s = 16$, and the domain is split, with the poroelastic medium on the left and the elastic one on the right. The height of the interface is 34.2, and the areas of Ω^{P} and Ω^{E} are 656.88 and 783.12, respectively. The left edge of the membrane is kept clamped and on it we also set zero fluid pressure; on the right edge of the membrane we impose the upward-pointing traction $\boldsymbol{t} = \frac{1}{\lambda^{\mathrm{E}}+2\mu^{\mathrm{E}}}(0,1/16)^{\mathrm{t}}$ that produces a resulting load of magnitude 1, and on the top and bottom edges we set a zero traction condition, together with zero-fluxes for the fluid pore pressure. We vary the Poisson ratio on each subdomain, whereas the remaining elastic parameters are taken as in the classical Cook's membrane benchmark, and the

TABLE 5.2

Test 5. Left: displacement of Cook's membrane at the top-right point (48,60) *for different values of the Poisson ratio. Right: numerical solutions produced with* $k = 1$ *and* $\nu^{\mathrm{E}} = \nu^{\mathrm{P}} = 0.49999$ *and plotted on the deformed domain.*

Displacement varying $\nu^{\mathrm{E}} = \nu^{\mathrm{P}}$		
$\nu^{\mathrm{E}} = \nu^{\mathrm{P}}$	$\boldsymbol{u}_1(48,60)$	$\boldsymbol{u}_2(48,60)$
0.49	–13.9273	18.9667
0.499	–13.8576	18.9546
0.4999	–13.8404	18.9513
0.49999	–13.8391	18.9506
0.499999	–13.8389	18.9505
Displacement with fixed $\nu^{\mathrm{P}} = 0.3$		
ν^{E}	$\boldsymbol{u}_1(48,60)$	$\boldsymbol{u}_2(48,60)$
0.49	–8.55342	11.7082
0.499	–8.33403	11.3576
0.4999	–8.31657	11.3101
0.49999	–8.31171	11.3015
0.499999	–8.31077	11.3002



material parameters for the fluid are set follows:

$$E^{\mathrm{E}} = E^{\mathrm{P}} = 1, \quad \alpha = 0.1, \quad \xi = 0.001, \quad \kappa = 10^{-6}, \quad c_0 = 0.01, \quad s_0 = 0.$$

We employ a mesh with 100 points per edge, representing 275,155 DoFs for the scheme with $k = 1$. As usual, we compute the displacements on the top-right corner of the membrane and collect the obtained values listed in Table 5.2. We perform two sets of simulations, one varying $\nu^{\mathrm{E}} = \nu^{\mathrm{P}}$ and the other keeping $\nu^{\mathrm{P}} = 0.3$ fixed and varying ν^{E} approaching the value $1/2$. Even if the near incompressibility of the poroelastic-elastic regimes can induce volumetric locking, together with spurious oscillations in the fluid pressure [38, 44], the solutions obtained in our tests clearly reveal the robustness of the formulation, at least with respect to the maximum dilation moduli between those on each subdomain (which in this case corresponds to that in the elastic domain). We also plot examples of the obtained numerical solutions, showing a deformation of the interface and distributions of the pore pressure and of all other individual field variables.

Acknowledgments. We express our sincere thanks to Marco Favino (Lausanne) for kindly providing the surface and volumetric meshes employed in Test 4, generated from micro-CT scanner images. We also thank two anonymous referees for constructive criticism which helped to improve the presentation and clarity of the manuscript.

REFERENCES

[1] Y. ACHDOU, R. GLOWINSKI, AND O. PIRONNEAU, *Tuning the mesh of a mixed method for the stream function. Vorticity formulation of the Navier-Stokes equations*, Numer. Math., 63 (1992), pp. 145–163.

[2] M. Alvarez, G. N. Gatica, and R. Ruiz-Baier, *A vorticity-based fully-mixed formulation for the 3D Brinkman-Darcy problem*, Comput. Methods Appl. Mech. Engrg., 307 (2016), pp. 68–95.

[3] V. Anaya, A. Bouharguane, D. Mora, C. Reales, R. Ruiz-Baier, N. Seloula, and H. Torres, *Analysis and approximation of a vorticity-velocity-pressure formulation for the Oseen equations*, J. Sci. Comput., 80 (2019), pp. 1577–1606.

[4] V. Anaya, Z. De Wijn, D. Mora, and R. Ruiz-Baier, *Mixed displacement-rotation-pressure formulations for linear elasticity*, Comput. Methods Appl. Mech. Engrg., 344 (2019), pp. 71–94.

[5] V. Anaya, B. Gómez-Vargas, D. Mora, and R. Ruiz-Baier, *Incorporating variable viscosity in vorticity-based formulations for Brinkman equations*, C. R. Math. Acad. Sci. Paris, 357 (2019), pp. 552–560.

[6] S. Atluri and A. Cazzani, *Rotations in computational solid mechanics*, Arch. Comput. Methods Engrg., 2 (1995), pp. 49–138.

[7] L. Berger, R. Bordas, D. Kay, and S. Tavener, *Stabilized lowest-order finite element approximation for linear three-field poroelasticity*, SIAM J. Sci. Comput., 37 (2015), pp. A2222–A2245, https://doi.org/10.1137/15M1009822.

[8] C. Bernardi and N. Chorfi, *Spectral discretization of the vorticity, velocity, and pressure formulation of the Stokes problem*, SIAM J. Numer. Anal., 44 (2006), pp. 826–850, https://doi.org/10.1137/050622687.

[9] F. Brezzi and M. Fortin, *Mixed and Hybrid Finite Element Methods*, Springer-Verlag, Berlin, 1991.

[10] M. Bukač, I. Yotov, R. Zakerzadeh, and P. Zunino, *Partitioning strategies for the interaction of a fluid with a poroelastic material based on a Nitsche's coupling approach*, Comput. Methods Appl. Mech. Engrg., 292 (2015), pp. 138–170.

[11] S. Chaillat, M. Darbas, and F. Le Louër, *Approximate local Dirichlet-to-Neumann map for three-dimensional time-harmonic elastic waves*, Comput. Methods Appl. Mech. Engrg., 297 (2015), pp. 62–83.

[12] C. D'Angelo and P. Zunino, *Robust numerical approximation of coupled Stokes' and Darcy's flows applied to vascular hemodynamics and biochemical transport*, ESAIM M2AN, 45 (2011), pp. 447–476.

[13] O. Daube, J.-L. Guermond, and A. Sellier, *Sur la formulation vitesse-tourbillon des équations de Navier-Stokes en écoulement incompressible*, C. R. Acad. Sci. Paris Sér. II, 313 (1991), pp. 377–382.

[14] G. de Boer, R. Hewson, M. Bryant, and D. Dowson, *An investigation into the contact between soft elastic and poroelastic bodies rotating under load*, Tribology Materials Surfaces Interfaces, 11 (2017), pp. 193–201.

[15] E. J. Dean, R. Glowinski, and O. Pironneau, *Iterative solution of the stream function-vorticity formulation of the Stokes problem, applications to the numerical simulation of incompressible viscous flow*, Comput. Methods Appl. Mech. Engrg., 87 (1991), pp. 117–155.

[16] F. Dubois, M. Salaün, and S. Salmon, *First vorticity–velocity–pressure numerical scheme for the Stokes problem*, Comput. Methods Appl. Mech. Engrg., 192 (2003), pp. 4877–4907.

[17] A. Ern, *Vorticity-velocity formulation of the Stokes problem with variable density and viscosity*, C. R. Acad. Sci. Paris Sér. I Math., 323 (1996), pp. 1159–1164.

[18] M. Favino, C. Gross, M. Drolshagen, L. Keilig, J. Deschner, C. Bourauel, and R. Krause, *Validation of a heterogeneous elastic-biphasic model for the numerical simulation of the PDL*, Comput. Methods Biomech. Biomed. Engrg., 16 (2013), pp. 544–553.

[19] A. Furtsev, H. Itou, and E. Rudoy, *Modeling of bonded elastic structures by a variational method: Theoretical analysis and numerical simulation*, Int. J. Solids Structures, 182/183 (2020), pp. 100–111.

[20] G. N. Gatica, *A Simple Introduction to the Mixed Finite Element Method: Theory and Applications*, Springer-Verlag, Berlin, 2014.

[21] G. N. Gatica, N. Heuer, and S. Meddahi, *On the numerical analysis of nonlinear twofold saddle point problems*, IMA J. Numer. Anal., 23 (2003), pp. 301–330.

[22] G.-M. Gie and J. P. Kelliher, *Boundary layer analysis of the Navier-Stokes equations with generalized Navier boundary conditions*, J. Differential Equations, 253 (2012), pp. 1862–1892.

[23] V. Girault, G. Pencheva, M. F. Wheeler, and T. Wildey, *Domain decomposition for poroelasticity and elasticity with DG jumps and mortars*, Math. Models Methods Appl. Sci., 21 (2011), pp. 169–213.

[24] V. Girault and P.-A. Raviart, *Finite Element Methods for Navier-Stokes Equations: Theory and Algorithms*, Springer Ser. Comput. Math. 5, Springer-Verlag, Berlin, 1986.

[25] V. Girault, M. F. Wheeler, T. Almani, and S. Dana, *A priori error estimates for a discretized poro-elastic–elastic system solved by a fixed-stress algorithm*, Oil Gas Sci. Tech., 74 (2019), 24.

[26] R. Glowinski and O. Pironneau, *Numerical methods for the first biharmonic equation and for the two-dimensional Stokes problem*, SIAM Rev., 21 (1979), pp. 167–212, https://doi.org/10.1137/1021028.

[27] C. Goll, T. Wick, and W. Wollner, *DOpElib: Differential equations and optimization environment; a goal oriented software library for solving PDEs and optimization problems with PDEs*, Arch. Numer. Software, 5 (2017), pp. 1–14.

[28] P. Göransson, *Tailored acoustic and vibrational damping in porous solids – Engineering performance in aerospace applications*, Aerospace Sci. Tech., 12 (2008), pp. 26–41.

[29] J. Heys, T. Manteuffel, S. McCormick, and J. Ruge, *First-order system least squares (FOSLS) for coupled fluid-elastic problems*, J. Comput. Phys., 195 (2004), pp. 560–575.

[30] J. S. Howell and N. J. Walkington, *Inf–sup conditions for twofold saddle point problems*, Numer. Math., 118 (2011), pp. 663–693.

[31] A. Ibrahimbegovic, *Finite elastic deformations and finite rotations of* $3d$ *continuum with independent rotation field*, Rev. Européenne Élém. Finis, 4 (1995), pp. 555–576.

[32] S. Kumar, R. Oyarzúa, R. Ruiz-Baier, and R. Sandilya, *Conservative discontinuous finite volume and mixed schemes for a new four-field formulation in poroelasticity*, ESAIM M2AN, 54 (2020), pp. 273–299.

[33] J. J. Lee, K.-A. Mardal, and R. Winther, *Parameter-robust discretization and preconditioning of Biot's consolidation model*, SIAM J. Sci. Comput., 39 (2017), pp. A1–A24, https://doi.org/10.1137/15M1029473.

[34] H. I. Ling and H. Liu, *Deformation analysis of reinforced soil retaining walls—Simplistic versus sophisticated finite element analyses*, Acta Geotechnica, 4 (2009), pp. 203–213.

[35] T. Merlini, *A variational formulation for finite elasticity with independent rotation and Biot-axial fields*, Comput. Mech., 19 (1997), pp. 153–168.

[36] T. Merlini and M. Morandini, *The helicoidal modeling in computational finite elasticity, part* III: *Finite element approximation for non-polar media*, Int. J. Solids Structures, 42 (2005), pp. 6475–6513.

[37] A. Mikelić and M. F. Wheeler, *On the interface law between a deformable porous medium containing a viscous fluid and an elastic body*, Math. Models Methods Appl. Sci., 22 (2012), 1250031.

[38] R. Oyarzúa and R. Ruiz-Baier, *Locking-free finite element methods for poroelasticity*, SIAM J. Numer. Anal., 54 (2016), pp. 2951–2973, https://doi.org/10.1137/15M1050082.

[39] S. Rani and S. Rani, *Axisymmetric deformation of a poroelastic layer overlying an elastic half-space due to surface loading*, Geophys. J. Internat. 211 (2017), pp. 883–896.

[40] R. Rannacher and R. Scott, *Some optimal error estimates for piecewise linear finite element approximations*, Math. Comp., 38 (1982), pp. 437–445.

[41] V. Ruas, *Variational approaches to the two-dimensional Stokes system in terms of the vorticity*, Mech. Res. Comm., 18 (1991), pp. 359–366.

[42] K. Rurkowska and S. Langer, *Coupling elastic-poroelastic material in structure-borne sound modeling*, J. Acoust. Soc. Amer., 133 (2013), 3446.

[43] M. Serpilli, *Classical and higher order interface conditions in poroelasticity*, Ann. Solid Structur. Mech., 11 (2019), pp. 1–10.

[44] W. Sun, Z. Cai, and J. Choo, *Mixed Arlequin method for multiscale poromechanics problems*, Int. J. Numer. Methods Engrg., 111 (2017), pp. 624–659.

[45] T. Wick, A. H. Elsheikh, and M. F. Wheeler, *Parameter estimation for the coupled Biot-Lamé-Navier problem in subsurface modeling*, in Proceedings of the 47th US Rock Mechanics/Geomechanics Symposium 2013, Vol. 4, American Rock Mechanics Association, Alexandria, VA, 2013, pp. 3000–3006.

View publication stats